frontiers | Frontiers in Energy Research

ORIGINAL RESEARCH
published: 12 May 2022
doi: 10.3389/fenrg.2022.882182

Impact of Synthesis Method and Metal Salt Precursors on the CO_2 Adsorption Performance of Layered Double Hydroxides Derived Mixed Metal Oxides

*Li Anne Cheah, G. V. Manohara, M. Mercedes Maroto-Valer and Susana Garcia**

Research Centre for Carbon Solutions (RCCS), School of Engineering and Physical Sciences, Heriot-Watt University, Edinburgh, United Kingdom

Since the 1990s, Mg-Al layered double hydroxide- (LDH-) based mixed metal oxides (MMOs) have emerged as promising CO_2 capture sorbents. Despite the numerous attempts to improve these materials, the impact of the synthesis method and employed metal salt precursors on the properties of LDHs and MMOs remains unknown. In order to address this gap, the present study investigated how two common synthesis methods (i.e., co-precipitation and urea hydrolysis) and two different salt precursors (i.e., metal chlorides and metal nitrates) affected the physical properties of LDHs and CO_2 capture performance of derived MMOs at intermediate temperature (200°C). The true chemical composition of the LDH phase was confirmed by the lattice parameter "*a*", which reveals the Mg/Al ratios at the octahedral layers. The impact of synthesis methods and metal salt precursors was evaluated in terms of synthesis efficiency metrics (e.g., synthesis yield, purity, and percentage of unreacted reactants), and their relationship was studied with the CO_2 adsorption behavior of MMOs in different aspects (e.g., adsorption capacities, kinetics, and cyclic stability). Pure MgO was used as a reference to assess the cyclic stability of MMOs sorbents. It was found that the LDHs synthesized by the co-precipitation method are superior in terms of high synthesis yields (~100%), good LDH purity, high adsorption capacities, and kinetics. In contrast, the LDHs synthesized with the urea hydrolysis method are better in terms of cyclic stability but tend to have low synthesis yields (54%–81%) and LDH purity (containing many amorphous impurities of Al-based hydroxides).

Keywords: CO_2 capture, layered double hydroxide, mixed metal oxides, yield, precursors, synthesis method, cyclic stability, hydrotalcite

OPEN ACCESS

Edited by:
Greeshma Gadikota, Cornell University, United States

Reviewed by:
Moises Bastos-Neto, Federal University of Ceara, Brazil
Xiayi (Eric) Hu, Xiangtan University, China

****Correspondence:***
Susana Garcia
s.garcia@hw.ac.uk

Specialty section:
This article was submitted to Carbon Capture, Utilization and Storage, a section of the journal Frontiers in Energy Research

Received: *23 February 2022*
Accepted: *08 April 2022*
Published: *12 May 2022*

Citation:
Cheah LA, Manohara GV, Maroto-Valer MM and Garcia S (2022) Impact of Synthesis Method and Metal Salt Precursors on the CO_2 Adsorption Performance of Layered Double Hydroxides Derived Mixed Metal Oxides. Front. Energy Res. 10:882182. doi: 10.3389/fenrg.2022.882182

1 INTRODUCTION

Atmospheric carbon dioxide (CO_2) concentration has reached an alarming level (415 ppm) and is still rising due to CO_2 emitting human activities (Keeling et al., 1976). The latest Intergovernmental Panel on Climate Change (IPCC) special report on the impacts of global warming warns about the urgent need to reduce CO_2 emissions and recommends carbon capture and storage (CCS) as one of the necessary techniques to tackle this issue (IPCC, 2018). At present, the capture of CO_2 *via*

absorption is still expensive and known, which might cause environmental issues when employed at an industrial scale (e.g., solvent degradation and volatile gas emissions) (Dutcher et al., 2015). As another option, CO_2 capture by adsorption using solid sorbents presents a promising alternative route for more effective regeneration due to lower heat capacity, lesser waste generation, better cyclic stability, and potentially higher capture capacity (Glier and Rubina, 2013; Wang et al., 2014; Abanades et al., 2015). In addition, some solid sorbents can capture CO_2 at high temperatures (>100–1,000°C), so it can be retrofitted directly to existing industrial plants and eliminate the step to cool down hot flue gas, thus reducing the cost of CO_2 capture (Sjostrom and Krutka, 2010).

Among the solid sorbents, Mg-Al layered double hydroxide-(LDH-) based mixed metal oxides (MMOs) have received considerable attention due to their good CO_2 capture performance and relatively mild adsorption-regeneration window (200°C–500°C). LDHs are a unique class of layered materials consisting of alternating layers of double metal hydroxides sheet and charge balancing anion. The general formula is $[M^{2+}_{1-x}M^{3+}_{x}(OH)_2]^{x+}[A^{m-}_{x/m}]^{x-} \cdot nH_2O$, where M^{2+} and M^{3+} represent the di- and trivalent cations, A^{m-} is the anion, and x represents the mole fraction of trivalent cations at the hydroxide layers ($x = M^{3+}/M^{2+}+M^{3+}$) (Cavani et al., 1991). In mineralogy, natural-occurring LDHs are classified as members of the hydrotalcite supergroup, which are named after Mg-Al-CO_3 LDHs with the specific Mg/Al ratio of 3 ($x = 0.25$), that is, hydrotalcite, $Mg_6Al_2(OH)_{12}(CO_3^{2-}) \cdot 4H_2O$ (Mills et al., 2012). When thermally decomposed, the LDH layer structure collapses and forms well-mixed metal oxides with acidic/basic surface properties that are responsible for CO_2 adsorption and catalytic applications. Long-term CO_2 cyclic tests show that LDH-derived MMOs have the adequate working capacity, high CO_2 selectivity, resistance to sour gas (H_2S), mild regeneration temperature, tolerance to moisture, and cyclic stability up to 1,000 h (Selow et al., 2009; van Dijk et al., 2011). With the right combination of cation pair and feedstock, MMOs can even act as a CO_2 conversion catalyst to convert adsorbed CO_2 into useful products, such as methane and methanol (Arco et al., 1999; Fang et al., 2019; Hanif et al., 2019; Martins et al., 2019; Arstad et al., 2020; Zhang et al., 2020). This unique dual functionality of LDH-derived MMOs (i.e., CO_2 capture sorbent and conversion catalyst) makes them one of the most studied sorbent materials in the sorption enhanced reaction processes (SERP) to produce high purity hydrogen (Cunha et al., 2012; Chanburanasiri et al., 2013; Jansen et al., 2013; Dijkstra et al., 2018; Martins et al., 2019).

LDH precursors have a significant influence and often determine the CO_2 capture and reactivity of derived MMOs. Variables that affect the properties of LDHs (e.g., synthesis method, composition, structure, and surface area) are important to understand in order to design better MMOs for different applications. Among these variables, the synthesis method has arguably one of the most significant impacts and should be carefully selected at the beginning of the material development stage. For example, many LDHs were synthesized using the reconstruction and anion exchange methods. These methods are cumbersome and are not sustainable for producing LDHs at an industrial scale because they require multistep synthetic processes that are often not stoichiometric in nature and may produce many unwanted side products (He et al., 2005). Further to that, the formation of LDHs is also known as highly sensitive to synthesis conditions (Forano et al., 2013). LDHs derived from different synthesis methods will likely show wide differences in physical properties (Prinetto et al., 2000).

For CO_2 capture applications, LDHs were mainly synthesized by the co-precipitation method because it is the simplest preparation method and is amenable to scaling up (Theiss et al., 2016; Tichit et al., 2019). However, some recent studies have suggested the hydrothermal urea hydrolysis method as a better route to synthesize LDH based sorbents in order to avoid the presence of impurities and their effect on the overall CO_2 capture properties (Hibino and Ohya, 2009; Cross and Brown, 2010; Cheah et al., 2020). Indeed, MMOs synthesized from the co-precipitation and urea hydrolysis method have shown different CO_2 adsorption values (0.30–0.72 mmol/g) (Gao et al., 2013). Nevertheless, the selection of a promising CO_2 capture sorbent does not depend entirely on a single metric (i.e., CO_2 sorption capacity) (Drage et al., 2012). Other synthetic factors are equally important as they can cause sustainability and environmental concerns (e.g., nature of the reagents, condition of the synthesis reaction, atom efficiency/synthesis yield, reactant usage, toxicity, and the post-synthesis processes involved) (Sheldon, 2018). Several studies have reported the non-stoichiometry nature of both the co-precipitation and urea hydrolysis method in the synthesis of LDHs, but the exact implications are not widely understood (Prinetto et al., 2000; Hibino and Ohya, 2009; Kou et al., 2018). Additionally, the role of salt precursors is not clear as well. Both lab-scale and industrial-scale synthesis of LDHs employ soluble metal salts (i.e., nitrates and chlorides) as precursors to provide metal ions. However, their impacts on the properties and performance of the resultant LDHs and MMOs are seldom being discussed. A previous study has highlighted the different environmental impacts of effluents derived from different metal salt precursors and the need to consider this aspect (Ozsa et al., 2006).

Given the importance that LDHs and related materials have gained in recent years as CO_2 capture sorbents, further insights on the effect of the synthesis method and role of the metal salt precursors on the properties of LDHs, as well as the impact on the CO_2 capture properties of the resultant MMOs, are required. In this work, we address these gaps by employing the two widely used synthesis methods (co-precipitation and urea hydrolysis) to prepare Mg-Al-CO_3 LDHs with varied Mg/Al compositions (Mg/Al = 2, 3, and 4) and employing different salts precursor, metal nitrates, and metal chlorides. These synthesized LDHs are comprehensively characterized by techniques such as powder X-ray diffraction (PXRD), Fourier transform infrared (FTIR), and elemental analysis (ICP-OES). The true chemical composition of the synthesized LDH phase is determined using the lattice parameter "*a*". The lattice parameter "*a*" gives information about the metal–metal distance on the LDH crystal lattice and is directly proportional to the extent of isomorphic

substitution. Additionally, this is not affected by the presence of impurities. Therefore, we used the "*a*" parameter to arrive at the exact composition of the synthesized LDHs. The synthesis efficiency of different synthesis methods and salts precursors is evaluated by the yields, purity, and percentage of unreacted metal ions. The CO_2 adsorption performance (e.g., adsorption capacity, kinetics, and cyclic stability of the synthesized LDHs) is evaluated and correlated with the synthesis method.

2 MATERIALS AND METHODS

2.1 Materials

All the reagents for LDH synthesis were used as received, for example, $Mg(NO_3)_2{\cdot}6H_2O$ (ACROS Organics, ≥98.0%); $Al(NO_3)_3{\cdot}9H_2O$ (Fluka®, ≥98.0%); Na_2CO_3 (Fisher Chemical, SLR grade); $MgCl_2$ (Fluka®, ≥98.0%); $AlCl_3$ (Fluka®, ≥99.0%); urea (Sigma-Aldrich, ≥98.0%); and NaOH (Fisher Chemical, SLR grade). Deionized water (Milli-Q® Reference ultrapure water, type 1, resistivity = 18.2 MΩ cm at 25°C) was used throughout the experiment.

2.2 Preparation of Mg-Al-CO_3 LDHs

2.2.1 Urea Hydrolysis

The urea hydrolysis method used to prepare Mg-Al-CO_3 LDHs was based on a modified Costantino's method and targeted to synthesize 1 g of LDHs (Costantino et al., 1998). Mixed metal solutions containing $Mg(NO_3)_2{\cdot}6H_2O$ and $Al(NO_3)_3{\cdot}9H_2O$ were prepared in different molar Mg/Al ratios (2, 3, and 4), and deionized water was added to arrive at a final concentration of 0.25 M. Solid urea 3.3 times more than the total moles of metal ions (urea: Mg + Al = 3.3) was added to the same mixed metal solutions and then sealed in hydrothermal autoclave reactors. All the resultant reaction mixtures were then hydrothermally treated in an oven at 90°C for 48 h. The pH of the supernatant solution/mother liquor for all the urea hydrolysis samples was measured after cooling down to room temperature. After that, the hydrothermally treated solutions were then centrifuged and washed with 100 ml of water to recover the LDHs. The LDHs were dried overnight in an oven at 70°C. The same protocol was followed to prepare LDHs from metal chlorides ($MgCl_2$ and $AlCl_3$) instead of metal nitrates. The samples prepared by the urea hydrolysis method are labeled as UHXXY, where UH represents the urea hydrolysis method, XX is the metal salt used in the synthesis (CL or NI), and Y stands for the molar Mg/Al ratios used (2, 3, and 4).

2.2.2 Co-Precipitation

The employed co-precipitation method was based on Miyata's method and targeted to synthesize 1 g of Mg-Al-CO_3 LDHs (Miyata and Kumura, 1973). A mixed metal solution containing Mg^{2+} and Al^{3+} ions in a 2:1 ratio was prepared using metal nitrates ($Mg(NO_3)_2{\cdot}6H_2O$ and $Al(NO_3)_3{\cdot}9H_2O$), and deionized water was added to arrive at a final concentration of 0.5 M. Then, the mixed metal solution was added dropwise into a base solution containing Na_2CO_3 (500 ml). The amount of carbonate ions in the Na_2CO_3 solution was three times that of the moles of carbonate ions in 1 g of LDH. Prior to the addition, the Na_2CO_3 solution was heated to 70°C, and pH was kept constant at 10 (±0.02), with the addition of 1 N NaOH solution (4.5 g of sodium hydroxide per 100 ml distilled water) using an auto-titrator (Metrohm 907 Autotitrator) and continuous stirring (400 rpm). The same condition was maintained throughout the addition reaction (1 h). After that, the resultant LDHs were aged in the mother liquor at 70°C for 24 h without any stirring. Next, the LDHs were recovered by centrifugation, followed by washing with 150 ml of water. The LDHs were dried overnight in an oven at 70°C. All the steps were repeated to prepare LDHs with different Mg/Al ratios (2, 3, and 4). LDHs were also prepared using metal chlorides ($MgCl_2$ and $AlCl_3$) instead of metal nitrates while keeping all other experimental conditions unchanged. The samples prepared by the co-precipitation method were labeled as CPXXY, where CP represents the co-precipitation method, XX stands for the metal salt used in the synthesis (chloride, CL or nitrate, NI), and Y is the molar Mg/Al ratios used (2, 3, and 4).

2.2.3 Preparation of Mg-Al-CO_3 Derived MMOs

The MMOs samples were prepared by calcining as-prepared LDHs at 400°C for 4 h in a furnace, using a ramping rate of 5°C/min under N_2 gas flow (purity 99.99%, 50 ml/min, oxygen-free).

2.3 Characterization

Powder X-ray diffraction patterns (PXRD) were recorded on a Bruker D8 Advance powder diffractometer, using Cu-K_α radiation (λ = 1.5406 Å), and data were collected over an angular range of 5–85°2 θ (1 h span; step size = 0.009°2 θ per second). Fourier transform infrared (FTIR) spectra were measured in the range of 4,000 to 600 cm^{-1} with 4 cm^{-1} resolution using a Perkin Elmer frontier IR single-range spectrometer under ATR mode. Elemental analysis (ICP-OES) was carried out by atomic emission spectra using Perkin Elmer Optima 5300DV. The LDH solid samples for elemental analysis were prepared by dissolving 30 mg of LDHs in concentrated sulphuric acid and diluting them with 25 ml of deionized water prior to analysis. The elemental analysis (ICP-OES) of the filtrate collected during the centrifugation of LDHs was analyzed without further dilution to check the presence of unreacted/leached-out metal ions. Morphology of the MMOs was characterized using the scanning electron microscopy (SEM) technique (JEOL JSM IT800). The gas adsorption/desorption experiments were carried out at 77 K using N_2 (ASAP 2420 V2.09). Prior to the gas adsorption experiments, the samples were degassed at 150°C for 2 h.

2.4 CO_2 Capture Studies

CO_2 adsorption tests were carried out in a thermal gravimetric analyzer (TA Instruments; TGA Discovery 5500; resolution: <0.1 μg, weighing precision: ±0.01%), and pristine LDHs were used to prepare MMOs to avoid CO_2 contamination. Approximately 50 mg of LDH powder was loaded into a platinum pan and decomposed under a continuous flow of pure N_2 gas (purity 99.998%, 50 ml/min, oxygen-free) at 400°C for 4 h, under ambient pressure (1 bar). The ramping rate was set

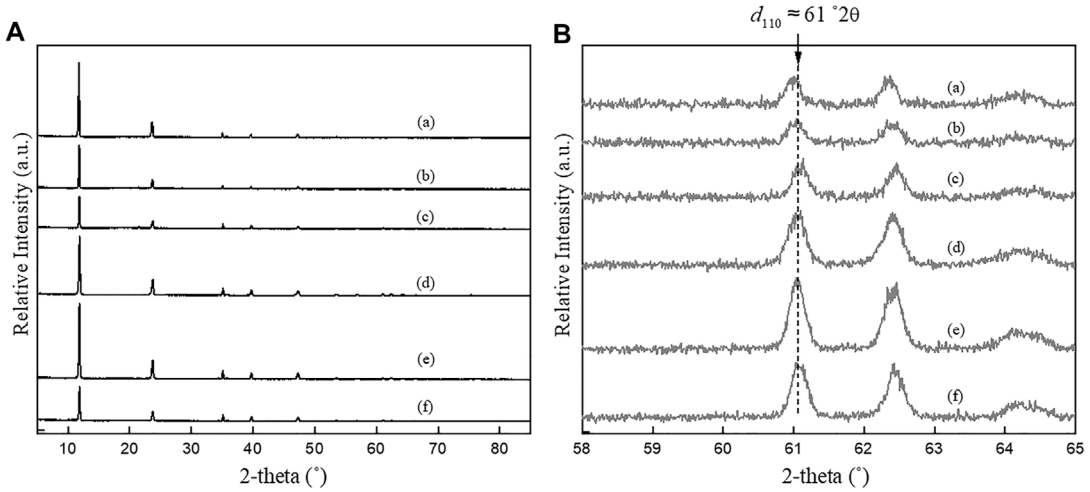

FIGURE 1 | PXRD patterns of LDHs synthesized using urea hydrolysis method in different nominal Mg/Al ratios and salt precursors between **(A)** 5–85 °2θ and **(B)** 58–65 °2θ. **(a)** UHNI2, **(b)** UHNI3, **(c)** UHNI4, **(d)** UHCL2, **(e)** UHCL3, and **(f)** UHCL4.

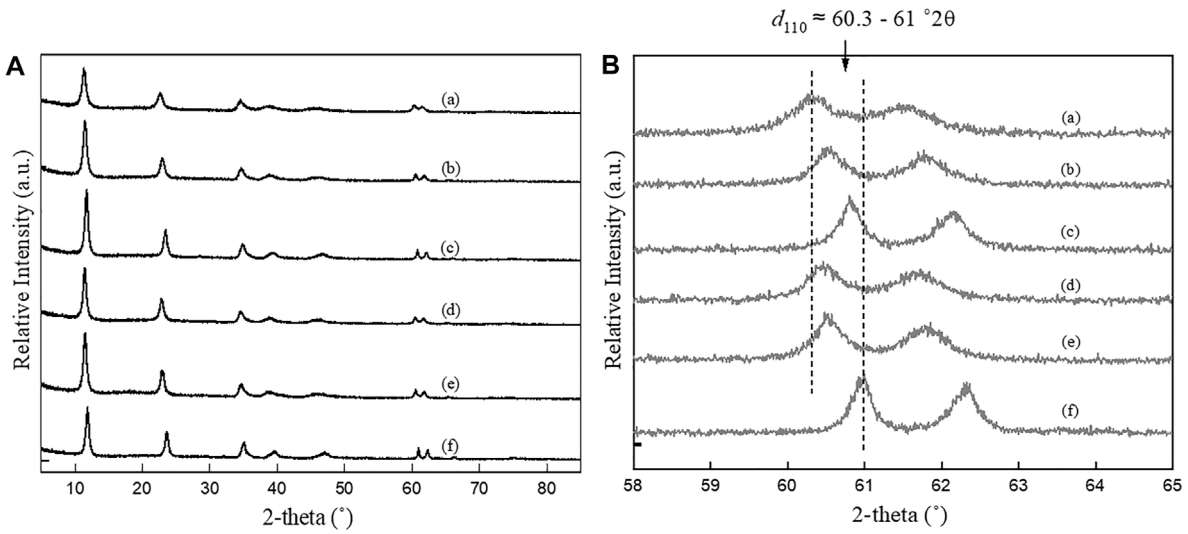

FIGURE 2 | PXRD patterns of LDHs synthesized using co-precipitation method in different nominal Mg/Al ratios and salt precursors between **(A)** 5–85 °2θ and **(B)** 58–65 °2θ. **(a)** CPNI2, **(b)** CPNI3, **(c)** CPNI4, **(d)** CPCL2, **(e)** CPCL3, and **(f)** CPCL4.

at 5°C/min. Once the decomposition was complete, the temperature was brought down to the desired temperature (200°C) and held for 10 min. After that, CO_2 gas flow (purity 99.98%, 80% v/v, diluted with N_2 gas purity 99.998%) was introduced for 2 h, and the CO_2 uptake capacity of MMOs was recorded.

For the cyclic test, fresh MMOs were prepared using the same protocol above and brought down to the desired temperature for CO_2 adsorption. The adsorption cycles were performed at 200°C for 30 min under CO_2 gas flow (purity 99.98%, 80% v/v, diluted with N_2 gas purity 99.998%), whereas the regeneration/desorption cycles were carried out at 400°C for 30 min, under pure N_2 gas flow (purity 99.998%, 100% v/v). The same CO_2 adsorption and regeneration step are repeated until 10 cycles are completed.

3 RESULTS AND DISCUSSION

3.1 Impact of Synthesis Method and Precursor Salts on Mg-Al-CO_3 LDHs

3.1.1 PXRD and FTIR Characterization

Figures 1 and **2** show the PXRD patterns of as-synthesized samples and reveal the successful synthesis of Mg-Al-CO_3

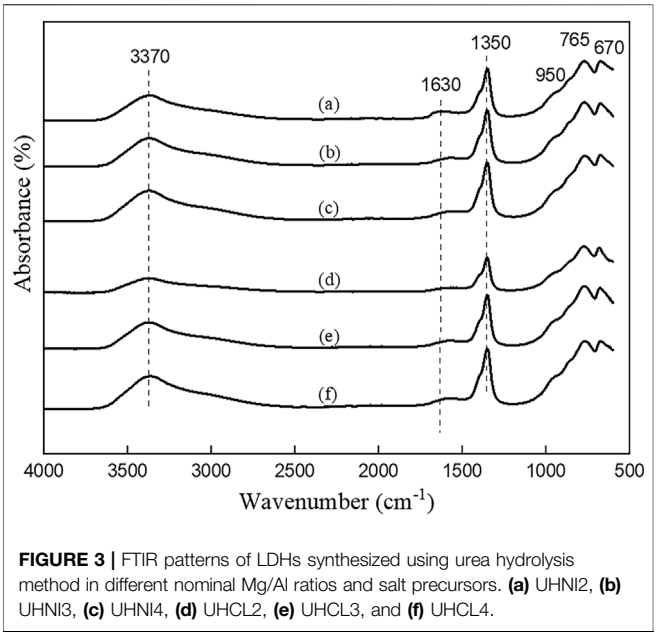

FIGURE 3 | FTIR patterns of LDHs synthesized using urea hydrolysis method in different nominal Mg/Al ratios and salt precursors. **(a)** UHNI2, **(b)** UHNI3, **(c)** UHNI4, **(d)** UHCL2, **(e)** UHCL3, and **(f)** UHCL4.

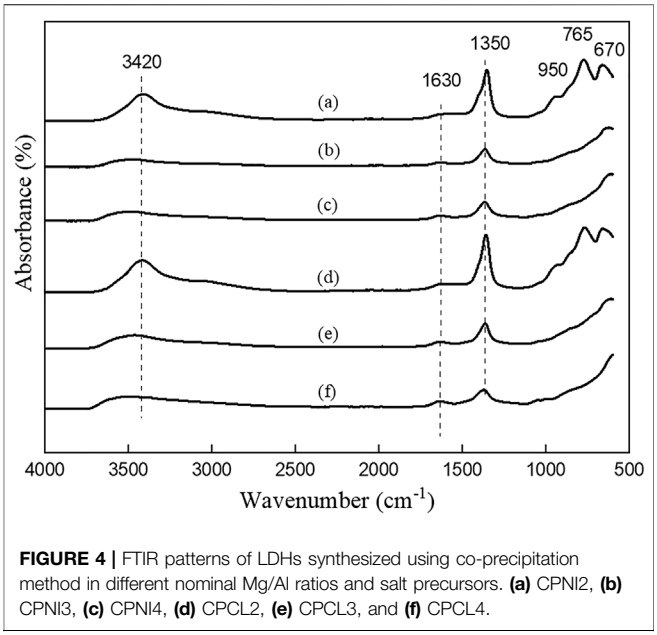

FIGURE 4 | FTIR patterns of LDHs synthesized using co-precipitation method in different nominal Mg/Al ratios and salt precursors. **(a)** CPNI2, **(b)** CPNI3, **(c)** CPNI4, **(d)** CPCL2, **(e)** CPCL3, and **(f)** CPCL4.

LDHs using the co-precipitation and urea hydrolysis methods with different nominal Mg/Al ratios and different metal salt precursors. The characteristic peaks of LDH are clearly seen in all the samples and match the *d*-values of the carbonate intercalated LDH system (i.e., 7.60, 3.80, 1.53, and 1.50 Å) (Allmann and Jepsen, 1969; Cavani et al., 1991). For example, the sharp, intense peak at a low 2θ value (~11.5°2θ) that yields *d*-values between 7.45 and 7.80 Å for different Mg/Al LDHs represents the interlayer distance between two successive metal hydroxide layers (d_{003}) and is the characteristic value for carbonate intercalated LDHs. The two "saw-tooth" shaped peaks at high 2θ value (60–62°2θ) correspond to 2*d* reflections of the LDHs and give the information across the *ab* plane.

The first peak of the "saw-tooth" in **Figures 1** and **2** gives the average *d*-value of 1.52 Å, and that corresponds to the average metal-oxygen distance at the hydroxide layers in the *(110)* plane ($d_{110} = d$ (M-O)), is related to the lattice parameter *a* of LDH ($a = 2 \times d_{110}$). PXRD patterns of the urea hydrolysis samples show higher intensity peaks compared to the co-precipitated samples, indicating a better crystallinity and agreeing well with literature-reported data. However, the higher peak intensity of the basal reflections of urea hydrolysis LDHs caused the 2*d* reflections not clearly visible in **Figure 1A**.

Figures 1B and **2B** shows a close inspection of the (*110*) peak of LDHs synthesized by both co-precipitation and urea hydrolysis method, which have clearly indicated that the 2θ values have varied between 60.3 and 61.0 °2θ, resulting in a wide different *a*-value (3.032–3.067 Å). As described in the introduction, the lattice parameter *a* is a direct indicator of the true chemical composition of LDHs. This shows the clear impact of the synthesis method on the chemical composition of LDHs. Further discussion on the relationship between the synthesis method and lattice parameters (*a* and *c*) on the chemical composition of LDH is in the next section.

Further evidence of carbonate intercalation and successful synthesis of LDHs is observed from the FTIR spectra shown in **Figures 3** and **4**. All the vibrations observed in the samples match the characteristic of carbonate intercalated LDHs (Hernandez-Moreno et al., 1985). For example, all the samples show a broad peak centered around 3,400 cm^{-1}, corresponding to the hydrogen-bonded hydroxyl ions due to layered hydroxyls and intercalated water molecules. The strong vibration around 1,360 cm^{-1} represents the CO_3^{2-} ion at the interlayers. The stretching vibration at 1,630 cm^{-1} represents the bending mode of the water molecules present in the interlayer gallery. The vibrations below 1,000 cm^{-1} represent the metal-oxygen (M-O) and metal-metal (M-M) bonds at the hydroxide layers.

3.1.2 Chemical Composition

LDHs are known to obey Vegard's law, which means the lattice parameters of LDH are very sensitive to its chemical composition (i.e., Mg/Al ratio at the double hydroxide layers) (Brindley and Kikkawa, 1979; Richardson, 2013). The lattice parameter *a* of LDH corresponds to the average metal-metal distance *d* (M-M) at the octahedral sites of hydroxide layers and, therefore, can be obtained from the value of d_{110} measured from PXRD ($a = 2 \times d_{110}$). As Al^{3+} (0.53 Å) has a smaller octahedral ionic radius than Mg^{2+} (0.72 Å), the isomorphic substitution of Mg^{2+} by Al^{3+} directly affects the unit cell parameter *a* of LDHs and can indicate the Mg/Al ratio at the hydroxide layers. The effect of cation ionic radius is best elucidated using the single hydroxides as an example. For instance, the average cation–cation distance, *d* (Mg-Mg) in magnesium hydroxide, $Mg(OH)_2$ is 3.142 Å, whereas the average cation–cation distance, *d*(Al-Al) in aluminum hydroxide, $Al(OH)_3$ is 2.763 Å. For Mg-Al LDHs, only part of the Mg^{2+} was substituted by Al^{3+} (*x* usually varies between 0.15 and 0.33). Thus, the lattice *a*-values should lie within these two values (e.g., *d* (Al-Al) < *d* (Mg-Al) < *d* (Mg-Mg)). The same holds

TABLE 1 | Lattice parameters *a* and *c* of LDHs synthesized from the urea hydrolysis and co-precipitation methods.

Urea hydrolysis method			Co-precipitation method		
Sample ID	**Lattice parameter, *a* ± 0.001 (Å)**	**Lattice parameter, *c* ± 0.001 (Å)**	**Sample ID**	**Lattice parameter, *a* ± 0.001 (Å)**	**Lattice parameter, *c* ± 0.001 (Å)**
UHNI2	3.033	22.355	CPNI2	3.037	22.610
UHNI3	3.034	22.436	CPNI3	3.057	23.133
UHNI4	3.032	22.343	CPNI4	3.061	23.394
UHCL2	3.033	22.322	CPCL2	3.044	22.366
UHCL3	3.038	22.581	CPCL3	3.057	23.064
UHCL4	3.036	22.443	CPCL4	3.067	23.171

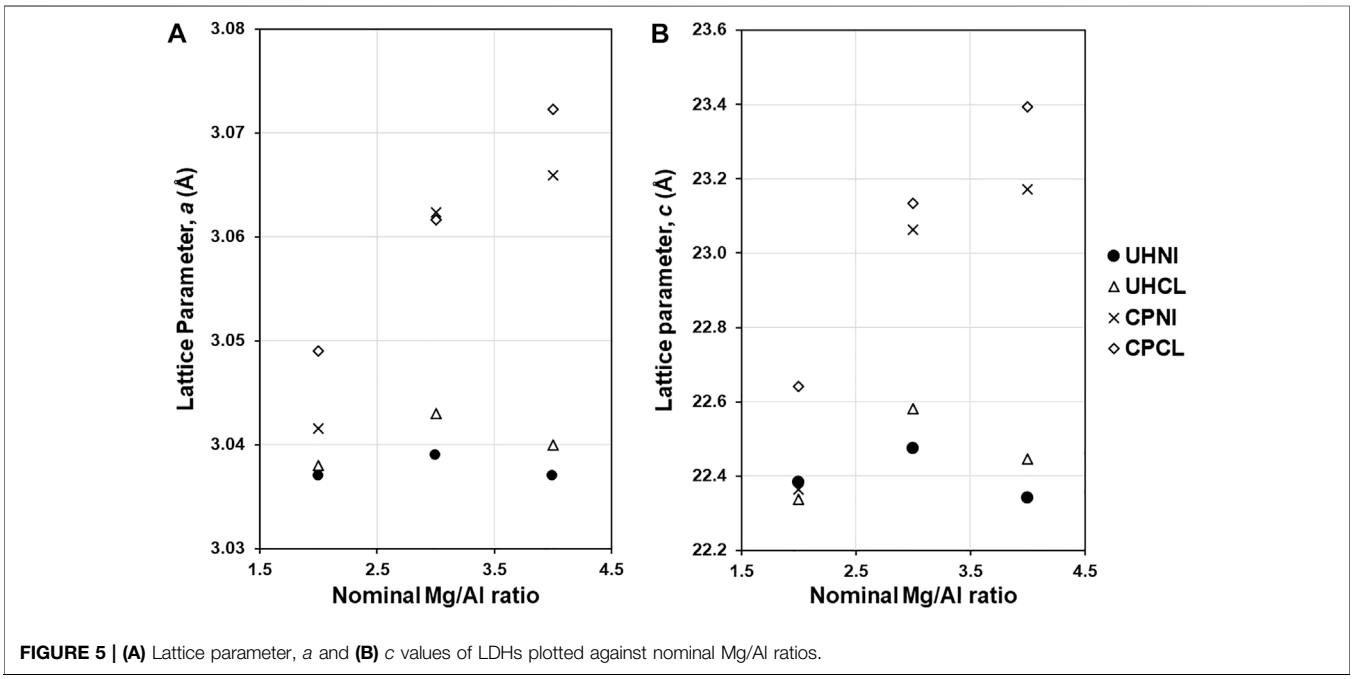

FIGURE 5 | (A) Lattice parameter, *a* and **(B)** *c* values of LDHs plotted against nominal Mg/Al ratios.

true for the lattice parameter *c*, which is the distance between three successive hydroxide layers, as the Coulombic attraction between successive metal hydroxide layers is affected by the number of Al^{3+} ions at the octahedral layers. However, unlike the lattice parameter *a*, the lattice parameter *c* is not entirely affected by chemical composition but also a number of other factors (e.g., the extent of hydration, the number, size, orientation of anions, and the strength of pseudo-bonds between anions and edge of hydroxide sheets) (Cavani et al., 1991; Marappa and Kamath, 2015). Thus, it is harder to predict the lattice parameter *c* from chemical composition alone. From PXRD, the lattice parameter *c* of LDHs is obtained from three times the value of d_{003} measured ($c = 3 \times d_{003}$).

The lattice parameters *a* and *c* of LDHs are given in **Table 1**, and their variation with the nominal Mg/Al ratios is shown in **Figures 5A,B**. The smaller *a*-values (3.033–3.038 Å) of LDHs synthesized by the urea hydrolysis method, compared to the co-precipitation method (3.037–3.067 Å), suggest a higher isomorphic substitution of Al^{3+} in the synthesized LDHs. Interestingly, the variation in the *a*-values is very small for the urea hydrolysis samples, irrespective of the nominal Mg/Al ratio and precursor metal salt employed. For example, the *a*-value (3.032 Å) of LDHs synthesized with a high nominal Mg/Al ratio (e.g., UHNI4) is very close to those synthesized using a lower nominal Mg/Al ratio (3.033–3.034 Å for UHNI2 and UHNI3). This indicates that the urea hydrolysis method generates LDHs with similar Mg/Al ratios, irrespective of their nominal ones.

Such findings are in good agreement with the literature reporting *a*-value of urea hydrolysis LDHs, which are usually reported as Al-rich LDHs, and the *a*-values are close to 3.04 Å (Adachi-Pagano et al., 2003; Benito et al., 2006; Radha et al., 2007; Gao et al., 2013). Nevertheless, it should be noted that most of these published urea hydrolysis LDHs follow the same procedure reported by Constatino et al. and use similar nominal composition (Mg/Al ratio = 2). Hence, it is not a surprise why these *a*-values are close to each other. This makes the observation of the fixed *a*-values found in the present work interesting as these nominal compositions (Mg/Al ratio of 3 and 4) were not studied

TABLE 2 | Synthesis yields for the co-precipitation and urea hydrolysis methods.

Urea hydrolysis method		Co-precipitation method	
Sample ID	**Synthesis yield (%)**	**Sample ID**	**Synthesis yield (%)**
UHNI2	81.2	CPNI2	96.0
UHNI3	66.7	CPNI3	100.9
UHNI4	57.0	CPNI4	100.9
UHCL2	77.0	CPCL2	94.9
UHCL3	67.1	CPCL3	99.6
UHCL4	54.3	CPCL4	100.7

in detail before, and it might provide a hint on the formation mechanism of LDH *via* urea hydrolysis method.

In contrast to the urea hydrolysis LDHs, the *a*-values of co-precipitated LDHs vary significantly (3.037–3.067 Å) and show a dependence on the nominal Mg/Al ratio used. This is more evident from the LDHs prepared by employing chloride salts (CPCL), which show a linear relationship between the *a* parameter and nominal Mg/Al ratio (**Figure 5A**). This confirms the progressive substitution of Al^{3+} ions into the crystal lattice of LDH and that the co-precipitation method can generate LDHs with different Mg/Al ratios. This observation is supported by the variation in the *c* parameter (**Figure 5B**), which shows a direct correlation between the *c*-parameter and nominal Mg/Al ratios. These findings are consistent with the literature observation of co-precipitated LDHs, where a wide range of *a*-values is reported (3.02–3.11 Å) (Gastuche et al., 1967; Kukkadapu et al., 1997; Kaneyoshi and Jones, 1999).

3.1.3 Synthesis Yield

The formation mechanism of LDHs *via* co-precipitation and urea hydrolysis method is as follows:

Co-precipitation method:

$$(1-x)\mathrm{Mg}^{2+}_{(aq)} + x\mathrm{Al}^{3+}_{(aq)} + \frac{x}{2}\mathrm{Na_2CO_3}_{(aq)} \xrightarrow{\text{NaOH, pH 10}} \mathrm{Mg_{1-x}Al_x(OH)_2(CO_3^{2-})_{x/2}} \cdot \left(1-\frac{3x}{2}\right)\mathrm{H_2O}_{(s)} + \mathrm{Na}^{+}_{(aq)}. \quad (1)$$

Urea hydrolysis method:

$$(1-x)\mathrm{Mg}^{2+}_{(aq)} + x\mathrm{Al}^{3+}_{(aq)} \xrightarrow{\text{Urea, 3.3 times the total moles of metal ions}} \mathrm{Mg_{1-x}Al_x(OH)_2(CO_3^{2-})_{x/2}} \cdot 1 - \frac{3x}{2}\mathrm{H_2O}_{(s)}. \quad (2)$$

The synthesis reaction yield is obtained by dividing the measured weight (i.e., actual yield) of the synthesized products over the expected weight (i.e., theoretical yield) of LDHs, calculated based on the stoichiometry reactions above and *x* derived from nominal Mg/Al ratios used at synthesis. The formula is presented in **Eq. 3**, and the results are tabulated in **Table 2**:

$$\textbf{Synthesis Yield}\ (\%) = \frac{\textbf{Actual Yield}\ (\mathbf{g})}{\textbf{Theoretical Yield}\,(\mathbf{g})} \times \mathbf{100}\%. \quad (3)$$

As shown in **Table 2**, not all the samples achieved 100% synthesis yield, and both synthesis methods show quite different results. For example, samples synthesized by the urea hydrolysis method show low yields, between 54% and 81%, whereas samples synthesized by the co-precipitation method show better yields, and some even reach a 100% yield. Interestingly, varying the nominal Mg/Al ratios seems to have a different effect on the resultant synthesis yield from both synthesis methods. For instance, when a larger nominal Mg/Al ratio (3 and 4) is employed to synthesize LDHs, the synthesis yield decreased for the urea hydrolysis method but increased for the co-precipitation method. On the contrary, employing different salt precursors does not show a large effect on the synthesis yields by both synthesis methods.

In order to understand this phenomenon, further insights into the formation mechanisms of LDHs by the employed synthesis methods are required. Broadly speaking, the formation/precipitation of LDHs from a solution of metal ions depends on the pH and solubility products of unitary hydroxides. For Mg-based LDHs, the precipitating pH can start from approximately 7.5 and remains stable up to pH 13 (Kukkadapu et al., 1997; Boclair and Braterman, 1999; Radha and Kamath, 2003; Seron and Delorme, 2008). **Table 3** shows that the final pH of most LDHs prepared is within the range of 7–10. Therefore, if the reaction is quantitative and follows the path described in **Eqs 1**, **2**, then the synthesis yield obtained should be equal to the theoretical yield (100%). However, this is clearly not the case, particularly with the urea hydrolysis samples. Interestingly, the LDHs synthesized with the lowest pH (UHNI2 and UHCL2) show higher yields than the rest with higher pH. This suggests another factor affecting the yields of LDHs, besides the pH condition.

Generally, the formation of LDHs competes with a series of side reactions. These reactions often produce secondary phases, which are usually metal hydroxides/oxy-hydroxides and carbonate species (Gastuche et al., 1967; Mascolo and Marino, 1980; Miyata, 1980; Pausch et al., 1986). For the urea hydrolysis method and at elevated temperatures (>80°C), urea hydrolyses in a two-step reaction, causing the pH of the reaction medium to gradually increase with time and produce ammonium (NH_4^+) and carbonate (CO_3^{2-}) as final products. During the process, Al-based hydroxides precipitate before Mg hydroxides because they have much lower solubility products and pH of formation, for example, Al hydroxides, $K_{sp} = 2 \times 10^{-31}$, pH ~ 4–6, and Mg hydroxides, $K_{sp} = 5.61 \times 10^{-12}$, pH ~ 9. However, due to the amphoteric nature of Al hydroxide, it redissolves before the pH where LDHs precipitates (i.e., dissolving at pH 6). It has been reported that the equilibrium between the dissolution of $Al(OH)_3$ and Mg-Al-LDHs can take up to 100 days to achieve (Johnson and Glasser, 2003). This means that it is possible that these precipitated Al hydroxide phases have not been completely dissolved or reprecipitated. This might explain the low synthesis yields of the urea hydrolysis method.

Further, the type of impurity phase formed will have a different effect on the resultant yield. For instance, the molecular weight of aluminum hydroxides, $Al(OH)_3$, is 78 g/mol, which is very close to the molecular weights of LDHs with different compositions (x = 0.25, 77.73 g/mol; x = 0.33, 78.18 g/mol). Therefore, when $Al(OH)_3$ is formed as an impurity phase along with the LDH, they are likely to compensate for the loss in percentage yield. The distinction between product weight and impurity weight becomes even more

TABLE 3 | Synthesis conditions of LDHs prepared from the urea hydrolysis and co-precipitation methods.

Sample ID	Mg/Al ratio	Metal salt precursor	Temperature (°C)	Precursor concentration (mol/dm^3)	Washing water volume (ml)	Aging Time (hours)	Final pH
UHNI2	2	Metal nitrates	90	0.25	100	48	7–8
UHNI3	3	Metal nitrates	90	0.25	100	48	8
UHNI4	4	Metal nitrates	90	0.25	100	48	8
UHCL2	2	Metal chlorides	90	0.25	100	48	7-8
UHCL3	3	Metal chlorides	90	0.25	100	48	8
UHCL4	4	Metal chlorides	90	0.25	100	48	8
CPNI2	2	Metal nitrates	70	0.25	150	24	10
CPNI3	3	Metal nitrates	70	0.25	150	24	10
CPNI4	4	Metal nitrates	70	0.25	150	24	10
CPCL2	2	Metal chlorides	70	0.25	150	24	10
CPCL3	3	Metal chlorides	70	0.25	150	24	10
CPCL4	4	Metal chlorides	70	0.25	150	24	10

complicated when the formed impurity is in an amorphous state since they are not easy to detect. On the contrary, the aluminum oxy-hydroxide, AlOOH, has a lower molecular weight (59.99 g/mol) that those for LDHs. If part of Al^{3+} is converted as AlOOH, then the resultant yield could reduce even if all Al^{3+} ions in the solutions are precipitated.

Although the co-precipitation method also follows a similar reaction, but pH is pre-calibrated to the condition where LDHs precipitate (i.e., pH = 10) and is well-controlled with the aid of an auto-titrator. This should technically minimize the chance of Al-based hydroxides being precipitated and is probably why close to theoretical yields (~100%) were obtained in all co-precipitation methods. Despite this, several studies reported that further characterization of co-precipitated samples with advanced techniques (e.g., solid-state ^{27}Al NMR) still found a small number of Al-based impurity phases (Rocha et al., 1999; Cadars et al., 2011; Cheah et al., 2020). Moreover, handling LDHs in the post-synthesis step may also cause variation in yield due to events such as leaching of metal cations from the crystal lattice, dissolution of LDHs during the aging, or incomplete removal of precipitation agents (e.g., sodium hydroxide/potassium hydroxide) (Cross and Brown, 2010; Jobbágy and Regazzoni, 2011; Iruretagoyena et al., 2015). This might explain why some co-precipitated samples have resultant yield less than or exceeding the theoretical 100% exceeding the theoretical 100%. All of this demonstrates the challenges in obtaining the information on the purity and the composition of LDHs based on observed yield alone. Hence, we demonstrate the necessity of the supplementary characterization techniques in arriving at the actual yield, purity, and composition of the LDHs.

Since the obtained synthesis yields do not distinguish between LDHs and impurities, elemental analysis of LDH samples and filtrate solutions was carried out to gain further insight into the composition.

3.2 Elemental Analysis (ICP-OES) of LDH Samples and Filtrates

Elemental analyses of Mg^{2+} and Al^{3+} ions precipitated in the samples (**Table 4**) and filtrate solution (**Table 5**) were carried out to have a comprehensive understanding of the LDH composition and synthesis yield.

3.2.1 Urea Hydrolysis Method

Table 4 reveals the observed Mg/Al ratios in the solid samples obtained from elemental analysis (ICP-OES) compared with their expected Mg/Al ratios at synthesis. All the urea hydrolysis samples show lower observed Mg/Al ratios (0.8–1.8) than their expected ones, suggesting a higher Al content in these samples. As described above, the minimum possible Mg/Al ratio in crystalline LDH is 2 ($x = 0.33$). Thus, the observation of these low observed Mg/Al ratios (0.8–1.8) indicates the presence of Al-based impurities in all urea hydrolysis samples. This result matches the hypothesis earlier proposed based on the LDH formation mechanism *via* the urea hydrolysis method and incomplete dissolution of Al-based hydroxides. The other strong evidence supporting this is the huge differences in observed Mg/Al ratios obtained from samples having similar *a*-values [e.g., UHNI4 (0.9) and UHNI2 (1.7)]. Similar *a*-values (3.032 Å) indicate those two samples have the same amount of Al^{3+} substitution in the LDH phase, but their observed Mg/Al ratios are not the same, which means they have a different Al content in the bulk phase. This clearly evidences the presence of impure Al phases in these samples. Their PXRD patterns (**Figures 1**, **2**) do not show any crystalline impurity phases, which corroborates the amorphous nature of the Al-based impurities.

The number of impure phases seems affected by the metal salt precursors employed, based on the different observed Mg/Al ratios obtained from the two methods (UHCL and UHNI). Those samples employing metal chlorides (UHCL) show larger observed Mg/Al ratios (1.3–1.8) than those measured for the UHNI samples, suggesting a higher Mg content. **Figures 1** and **2** show that no other crystalline phases apart from the LDH were detected in the PXRD patterns and amorphous Mg-based impure phases are not yet known; hence, this Mg-content should be measured directly from the LDH phase and could be used as an indication of LDH purity. Based on the close agreement between the expected and observed Mg/Al ratio of UHCL samples, metal chlorides seem to be a more effective precursor to produce high purity LDHs.

TABLE 4 | The expected (nominal), observed (bulk) Mg/Al ratios, and sodium content of LDHs synthesized from the urea hydrolysis and co-precipitation methods.

Urea hydrolysis method				Co-precipitation method			
Sample ID	Mg/Al ratios		Sodium content (wt %)	Sample ID	Mg/Al ratios		Sodium content (wt %)
	Expected	Observed			Expected	Observed	
UHNI2	2.0	0.9	0.16	CPNI2	2.0	2.7	0.91
UHNI3	3.0	0.8	0.22	CPNI3	3.0	3.0	0.65
UHNI4	4.0	1.7	0.19	CPNI4	4.0	4.0	0.53
UHCL2	2.0	1.3	0.13	CPCL2	2.0	2.2	0.34
UHCL3	3.0	1.6	0.19	CPCL3	3.0	3.0	0.48
UHCL4	4.0	1.8	0.04	CPCL4	4.0	4.0	0.40

TABLE 5 | Percentage of unreacted metal ions in the filtrates collected during the synthesis of LDHs using the urea hydrolysis and co-precipitation methods.

Urea hydrolysis method			Co-precipitation method		
Sample ID	Percentage unreacted (%)		Sample ID	Percentage unreacted (%)	
	Mg	Al		Mg	Al
UHNI2	57.5	0.0	CPNI2	0.1	8.6
UHNI3	73.9	0.0	CPNI3	0.0	0.2
UHNI4	56.8	0.0	CPNI4	0.1	0.3
UHCL2	33.6	0.1	CPCL2	0.0	2.3
UHCL3	45.6	0.4	CPCL3	0.1	0.2
UHCL4	55.3	0.1	CPCL4	0.1	0.2

Table 5 shows the percentage of unreacted metal ions measured in the filtrates of all samples collected from the washing step with respect to the nominal Mg/Al ratios at synthesis. It is observed that the number of Al^{3+} ions is negligible in all filtrates from the urea hydrolysis method, indicating that most Al^{3+} ions were precipitated. However, a large content of Mg^{2+} ions (34%–74% of the concentration of Mg^{2+} ions used at synthesis) is found in these filtrates, which evidenced the incomplete precipitation of these ions into LDHs. This also matches the earlier hypothesis that part of the precursors (Al^{3+}) is precipitated as impurities phases, rather than LDHs, which caused the low synthesis yields (54–81%) obtained from the urea hydrolysis method. Nevertheless, it is also possible that part of these Mg^{2+} ions is a result of leaching out from the LDH crystal lattice during the aging and/or washing stage of the urea hydrolysis method.

Again, the percentages of unreacted Mg^{2+} ions are lower in the filtrates of metal chlorides (UHCL) compared to the metal nitrates (UHNI). This agrees well with the earlier analysis of observed Mg/Al ratios and confirms that metal chlorides are a more effective precursor to precipitate metal ions into LDHs. However, although more metal ions (i.e., Mg^{2+}) have precipitated, the final product yield of UHCL samples is still lower than that for UHNI samples [e.g., UHCL2 (77.0%) and UHNI2 (81.2%)]. This proves the non-quantitative nature of the urea hydrolysis method and confirms the presence of a large amount of amorphous Al-based impurities phases in the UHNI samples. So far, all evidence present in this section matches with the previous solid-state ^{27}Al NMR studies of urea hydrolysis LDHs; the author found two different AlO_6 octahedral aluminum sites and implies that the amount of impurities phase can be significant, as the signal intensity due to impurities phase is as high as 37% relative to the intensity of pure LDHs (67%) (Vyalikh et al., 2009).

It is apparent now that the formation mechanism proposed for the urea hydrolysis method is mostly valid. However, it still needs an explanation for the fixed *a*-value observed in all urea hydrolysis samples. One explanation for this is that there exists a thermodynamic preference to synthesize LDHs of this composition ($a \sim 3.04$ Å) as the hydrothermal conditions are very close to the formation condition of naturally occurring LDHs.

Surprisingly, the elemental analysis revealed small amounts of sodium (0.04–0.22 wt%) in all urea hydrolysis samples. This is rather unanticipated because, unlike the co-precipitation method, the urea hydrolysis method does not involve any sodium precursors in the synthesis steps (e.g., NaOH and Na_2CO_3). All the samples were carefully handled, and containers were acid-washed prior to usage. Hence, the only possible source of this sodium content is from the metal salt precursors, where the sodium content was considered negligible due to the low concentration (10–100 mg/kg) in all reagents.

3.2.2 Co-Precipitation Method

Table 4 shows that the observed Mg/Al ratios of co-precipitated samples agree well with their expected values, which means the co-precipitation method can produce LDHs close to the desired compositions. The only two exceptions are samples CPNI2 and CPCL2, which were targeted to synthesize LDHs close to the upper limit of x (0.33). For the other compositions (Mg/Al ratios of 3 and 4), the good agreement between *a*-parameters, synthesis yields and observed Mg/Al ratios prove the higher LDH purity of the co-precipitated samples *versus* the urea hydrolysis ones.

A small amount of sodium content (0.34%–0.91%) was observed in all the co-precipitated LDHs, which may originate from the sodium precursors used in the synthesis (e.g., NaOH and Na_2CO_3). The employed washing protocol reduced the sodium content to a very small percentage (<1%) and explained why some of the synthesis yields of LDHs are slightly more than 100% (100.6%–100.9%). Further washing may cause the leaching out of metal ions from the LDH lattice, which can affect the final chemical composition of LDHs and risk sacrificing the synthesis yields. Therefore, we have not attempted to completely remove the sodium content but rather kept a consistent washing protocol for all samples.

Elemental analysis of the filtrates (**Table 5**) revealed the full conversion of reactants in the co-precipitation reaction as the number of metal ions (both Mg^{2+} and Al^{3+}) in the filtrates is almost zero in most of the samples. Only a small percentage of unreacted Al^{3+} ions was measured in the two samples, CPNI2 and CPCL2, consistent with their observed Mg/Al ratios (**Table 4**) and synthesis yields (**Table 2**).

When an Mg/Al ratio of 3 was used in the synthesis *via* the co-precipitation method, LDHs with a composition close to that of the mineral hydrotalcite ($Mg_6Al_2CO_3(OH)_{16}{\cdot}4H_2O$) were obtained. Both CPNI3 and CPCL3 showed the lowest content of unreacted Mg^{2+} and Al^{3+} ions in the filtrates, and their synthesis yields were closest to the ideal 100%. Both samples also showed *a*-parameter value (3.057 Å) that matches that of the mineral hydrotalcite (3.054 Å). The good agreement between yields, *a*-parameter, and observed Mg/Al ratio indicates that the reaction is quantitative. In contrast, syntheses targeting LDHs with other compositions show discrepancies in their *a*-parameters and yields.

3.3 Impact of Synthesis Method and Precursor Salts on MMOs

3.3.1 MMOs Sorbent Yields

All LDHs synthesized were subjected to thermal decomposition as described in the experimental section to obtain MMOs. PXRD patterns of the MMOs are shown in **Supplementary Figures S1, S2**. All the LDH characteristic peaks previously seen in PXRD patterns (**Figures 1**, **2**) have now disappeared and are replaced by three broad reflections corresponding to MgO with *d*-values of 2.43, 2.11, and 1.49 Å (Hazen, 1976). The formation of MMOs was further characterized by FTIR spectra, as shown in **Supplementary Figures S3, S4**. All the characteristic vibrations due to LDHs (e.g., 3,400, 1,630, and 1,360 cm^{-1}) were significantly reduced on the FTIR spectra of MMOs and showed different signals at 1,400 cm^{-1} and 1,540 cm^{-1}. In the literature, these two peaks are commonly seen in decomposed MMOs and are attributed to the adsorption of atmospheric water and CO_2 species. **Table 6** shows the percentage weight loss of MMOs during the thermal decomposition step. There is an experimental inconsistency of less than ±1% for percentage weight loss due to the heterogeneity of sample bulk.

The theoretical weight loss for complete dehydroxylation, dehydration, and deanation (i.e., removal of CO_3^{2-} anion at interlayer) of LDH with *x* between 0.15 and 0.33 is in the range of 43.9%–45.2%. As seen in **Table 6**, none of the MMOs samples have achieved the theoretical weight loss values, although their FTIR spectra confirm the complete decomposition of LDHs precursors. Among the two synthesis methods, the percentage of weight loss in the case of urea hydrolysis LDHs is lower (37%–41.7%) compared to the co-precipitated LDHs (39–42%). It is likely that the presence of impurity phases contributed to the discrepancies in weight loss.

TABLE 6 | Percentage loss of LDHs in the thermal decomposition step.

Sample ID	Percentage weight loss (%)	Sample ID	Percentage loss (%)
UHNI2	41.7	CPNI2	41.9
UHNI3	37.8	CPNI3	41.5
UHNI4	38.6	CPNI4	41.8
UHCL2	40.6	CPCL2	39.2
UHCL3	37.0	CPCL3	40.9
UHCL4	37.3	CPCL4	41.1

3.3.2 BET and SEM Analysis

Figures 6 and **7** show the nitrogen adsorption isotherms at 77 K of MMOs samples prepared by urea hydrolysis and co-precipitation method. Interestingly, both MMOs synthesized by different synthesis methods show different types of isotherms profiles. For example, all urea hydrolysis MMOs show type II isotherms, suggesting them as non-porous or macroporous materials, whereas co-precipitated MMOs show type IV isotherms, suggesting them as a microporous or mesoporous material. Hysteresis loops give more information about the textural properties of MMOs. For example, the narrow hysteresis loop of urea hydrolysis MMOs that ended in the middle of the isotherm is documented as usually caused by inter-particle capillary condensation and from material that is non-rigid plate-like particles. On the contrary, the co-precipitated MMOs exhibit a hysteresis loop only at the beginning of the desorption branch, suggesting they have more complex pore structures made up of interconnected networks of pores of varying sizes and shapes. **Figure 8** shows the calculated BET surface area using information from nitrogen adsorption isotherms at 77 K. It seems that the BET areas of co-precipitated MMOs are at least two times larger than the ones of urea hydrolysis MMOs.

Scanning electron microscopy (SEM) analysis was carried out to study the morphology of MMOs synthesized from the two synthesis methods. SEM micrographs of all MMOs samples are available in **Supplementary Figures S5–S8**. **Figures 9** and **10** present the morphology of all MMOs synthesized from the two synthesis methods. Overall, the SEM images obtained for urea hydrolysis MMOs (**Figure 9**) show large plate-like hexagonal crystallites with a couple of microns. On the contrary, MMOs obtained from the co-precipitated LDHs are large aggregates of crystallites with irregular shapes. A closer look at the surface of these co-precipitated MMOs can observe the decomposed sand-rose-like particles, whereas the surface of urea hydrolysis MMOs appears to be smooth under SEM examinations. This is perhaps why the BET areas of co-precipitated MMOs are larger than the urea hydrolysis MMOs (**Figure 8**). Thus far, the observed

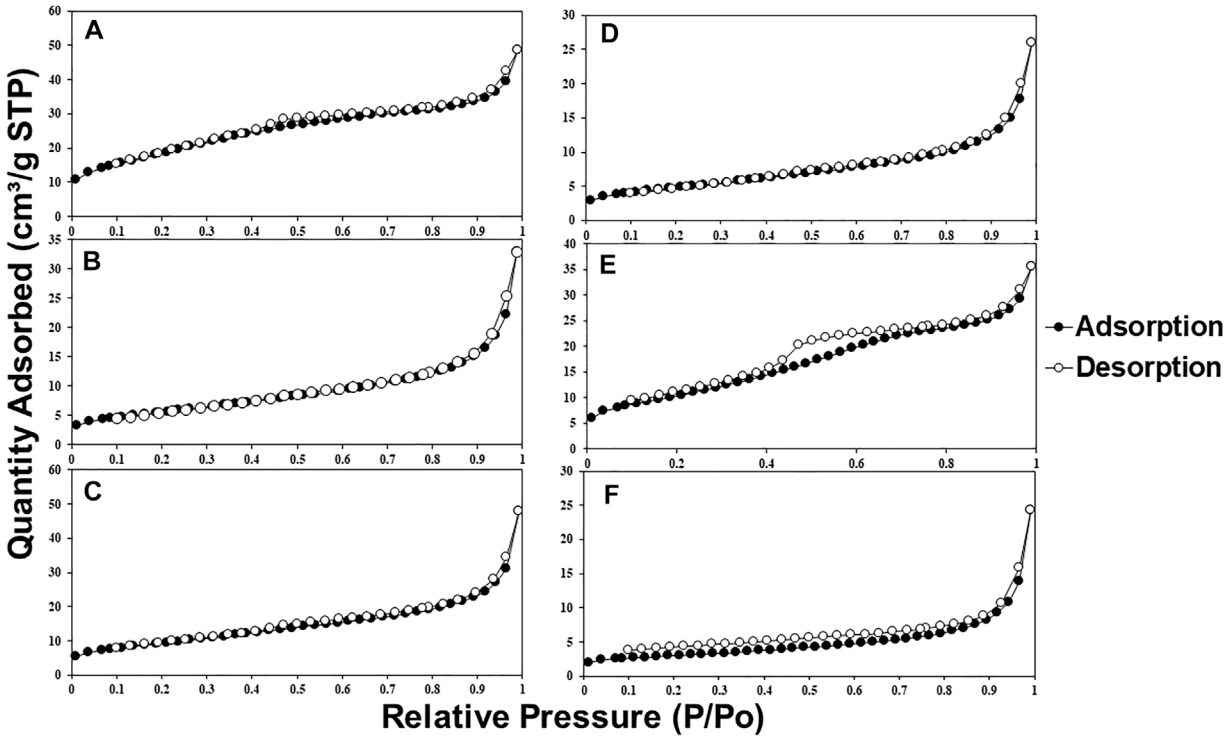

FIGURE 6 | Nitrogen adsorption isotherms (77 K) of MMOs synthesized by **(A)** UHNI2, **(B)** UHNI3, **(C)** UHNI4, **(D)** UHCL2, **(E)** UHCL3, and **(F)** UHCL4.

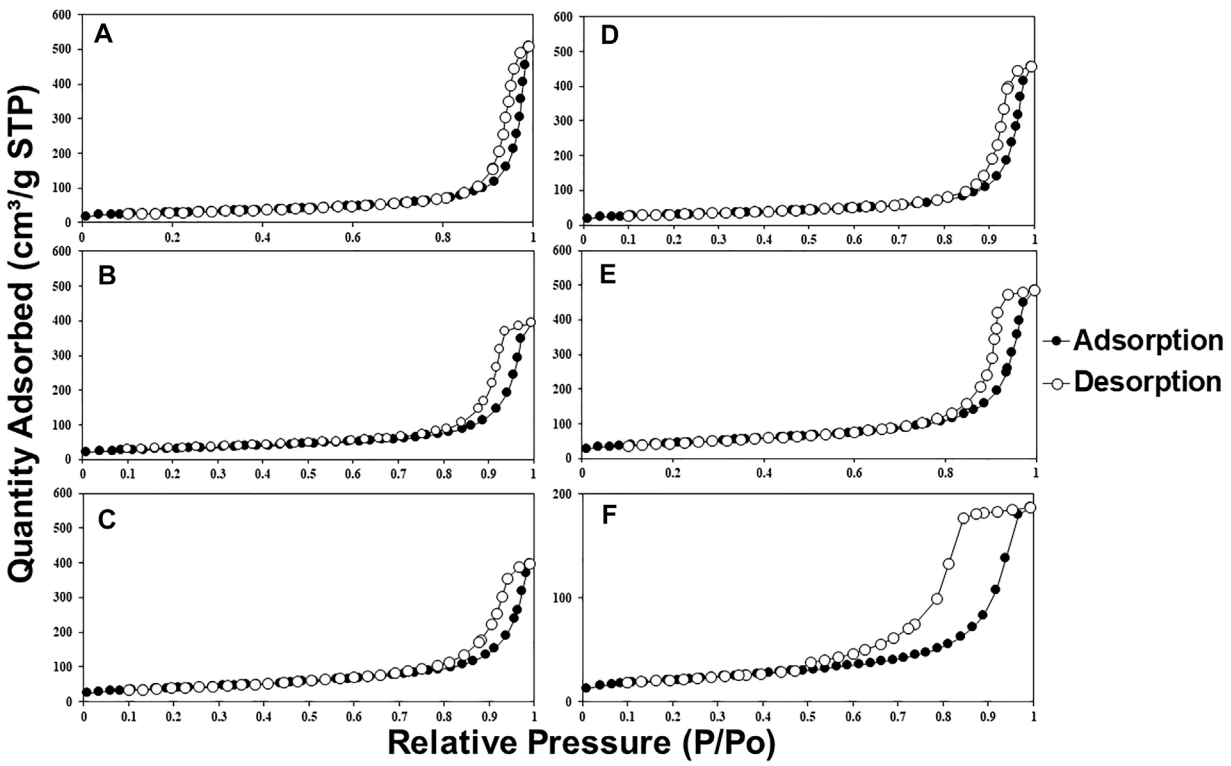

FIGURE 7 | Nitrogen adsorption isotherms (77 K) of MMOs synthesized by **(A)** CPNI2, **(B)** CPNI3, **(C)** CPNI4, **(D)** CPCL2, **(E)** CPCL3, and **(F)** CPCL4.

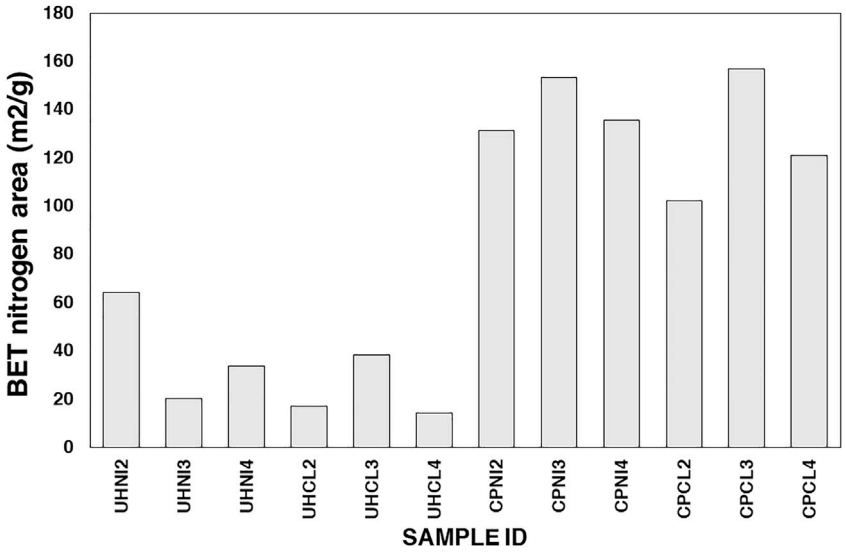

FIGURE 8 | BET surface areas of MMOs synthesized from the urea hydrolysis and co-precipitation methods.

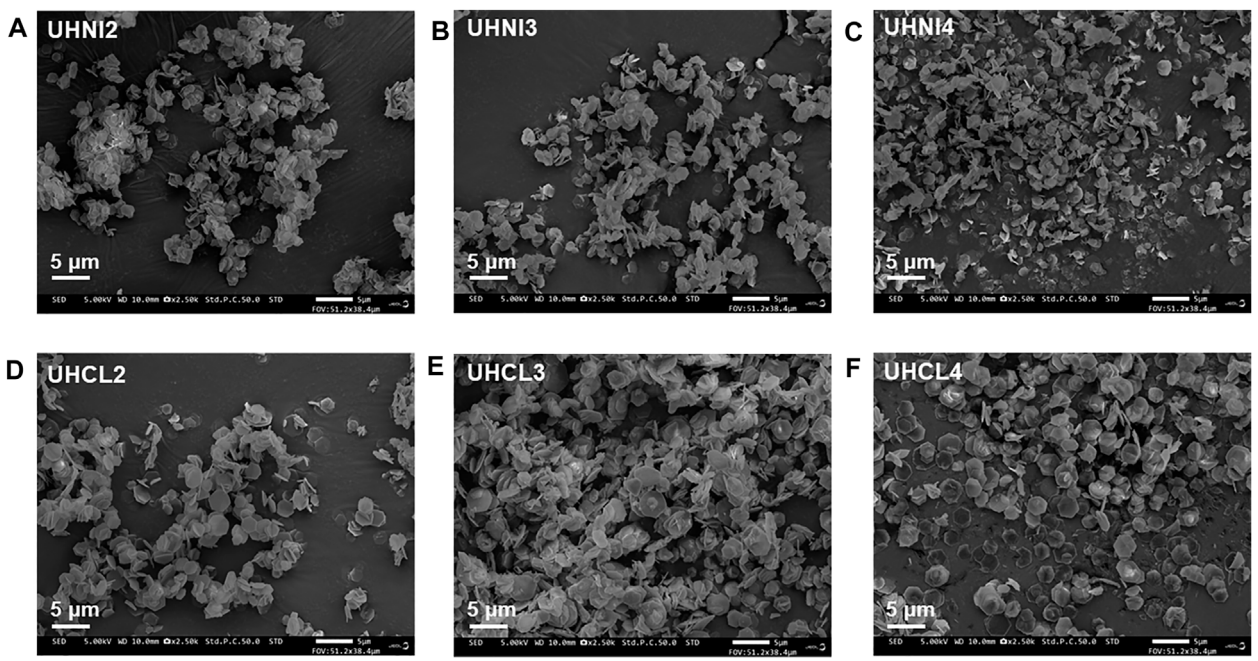

FIGURE 9 | SEM micrographs of MMOs synthesized with the urea hydrolysis method. **(A)** UHNI2, **(B)** UHNI3, **(C)** UHNI4, **(D)** UHCL2, **(E)** UHCL3, and **(F)** UHCL4.

morphologies for MMOs agree well with the nitrogen isotherms analyses above and literature reports.

3.4 CO_2 Adsorption Tests

3.4.1 CO_2 Adsorption Capacities

Figure 11 shows the CO_2 adsorption capacities measured for MMOs derived from LDHs synthesized in the present study at 200°C and CO_2 partial pressure of 0.8 bar (80% v/v). The observed Mg/Al ratios and sodium content of the LDHs are also plotted in **Figure 11** to investigate their relationship with the CO_2 adsorption capacities of derived MMOs. The error bars on the histogram represent the range of uncertainty due to the weighting precision of the thermogravimetric analyzer.

Figure 11 shows that the CO_2 adsorption capacities of MMOs obtained from the co-precipitation method (0.5–0.9 mmol/g) are generally higher than those obtained from the urea hydrolysis

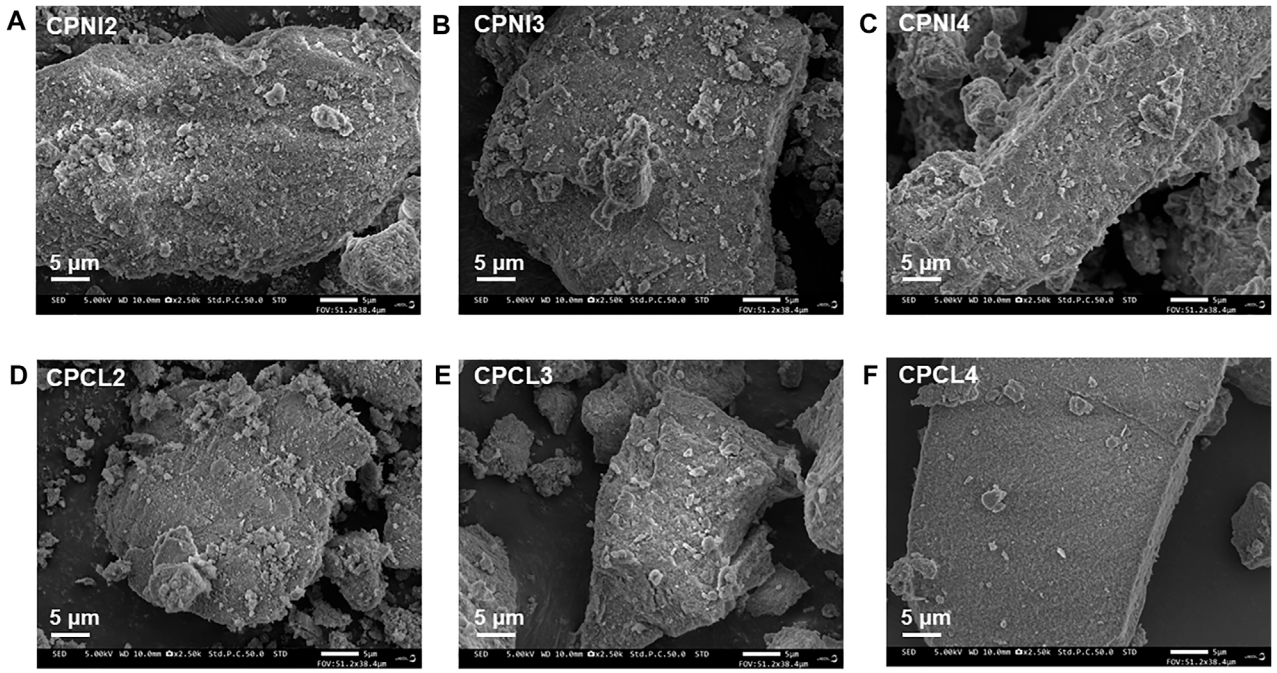

FIGURE 10 | SEM micrographs of selected MMOs synthesized with the co-precipitation method. **(A)** CPNI2, **(B)** CPNI3, **(C)** CPNI4, **(D)** CPCL2, **(E)** CPCL3, and **(F)** CPCL4.

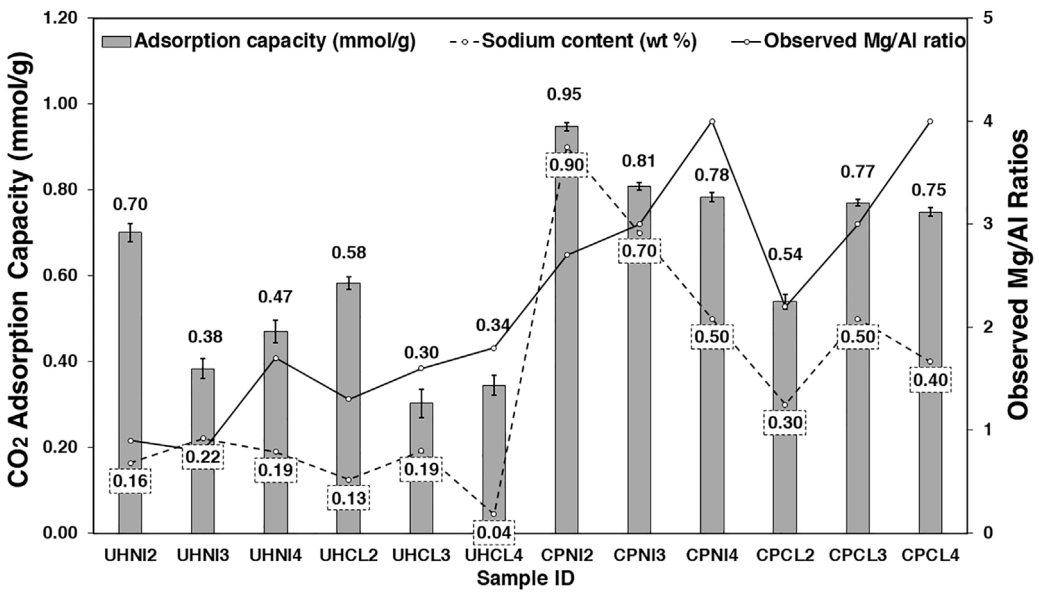

FIGURE 11 | CO_2 adsorption capacities of MMOs synthesized *via* urea hydrolysis and co-precipitation methods at 200°C, plotted against the observed (measured) Mg/Al ratios and sodium content.

method (0.3–0.7 mmol/g). The higher observed Mg/Al ratios (i.e., Mg content), sodium content, and surface area of co-precipitated MMOs are likely the factors causing their CO_2 adsorption values to be higher than the urea hydrolysis derived MMOs. Among these parameters, the CO_2 adsorption capacities of co-precipitated MMOs seem more strongly influenced by their sodium content. For example, the highest CO_2 adsorption capacities were recorded from samples CPNI2 and CPCL3, which also presented the highest sodium content. No clear correlation between BET surface area (**Figure 8**) and CO_2

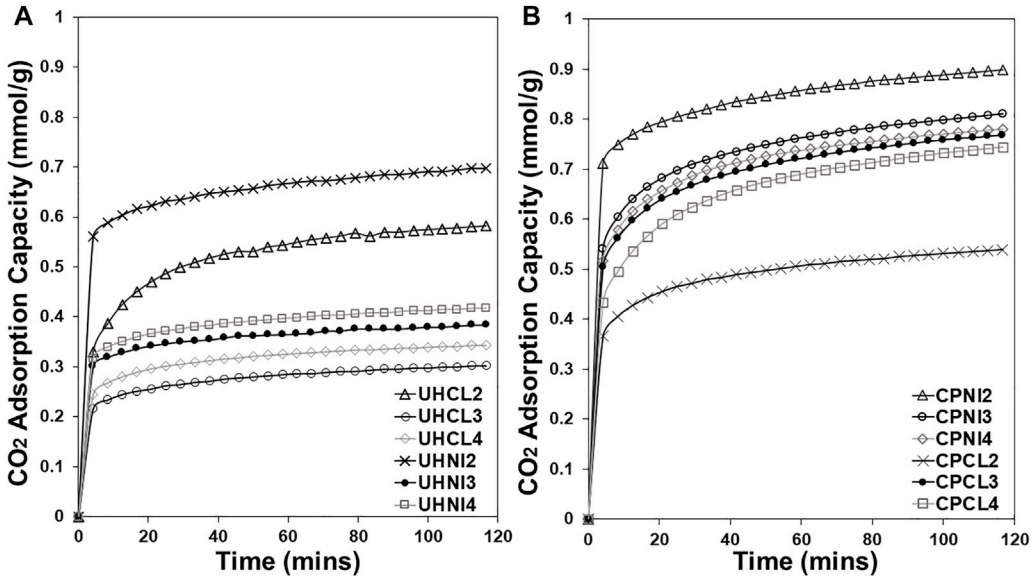

FIGURE 12 | CO_2 adsorption capacity *vs*. time (minutes) profile of MMOs derived by the LDHs synthesized by **(A)** urea hydrolysis and **(B)** co-precipitation methods.

amount adsorbed is seen. From **Figure 11**, the Mg/Al ratio of the co-precipitated sorbents (both crystal and bulk Mg/Al ratios) does not seem to have an obvious impact on the CO_2 adsorption capacities; that is, the samples with different *a*-values and observed Mg/Al ratios (CPNI3, CPNI4, CPCL3, and CPCL4) showed close values of CO_2 adsorption capacities (0.75–0.81 mmol/g). Coincidentally, these samples also showed similar synthesis yield values (~100%). Contrary to the synthesis method, different precursor salts do not play a major role in the CO_2 adsorption of MMOs. However, MMOs synthesized by metal nitrates show a slightly higher CO_2 adsorption capacity than those synthesized with metal chlorides in both synthesis methods. This is likely due to the higher sodium content in the precursor metal nitrates used to synthesize LDH samples.

In the case of urea hydrolysis derived MMOs, none of the metrics determined earlier (e.g., sodium content, observed Mg/Al ratios, and BET surface area) show an obvious correlation with their CO_2 amount adsorbed. However, a further investigation shows that the two highest CO_2 adsorption capacities were measured from the samples with the lowest observed Mg/Al ratios (e.g., UHNI2 and UHCL2). This means that the low LDH purity and presence of impurities in the urea hydrolysis samples may have played a role in this. For instance, despite having the lowest observed Mg/Al ratios, samples UHNI2 and UHCL2 showed the highest yields (81.2% and 77.0%) and the smallest deviation from expected Mg/Al ratios, which suggests they have the lowest number of impurities and high LDH purity. This is probably why they exhibit the highest CO_2 adsorption capacities among the urea hydrolysis derived MMOs. It is also possible that the impure phases have hindered the access of CO_2 to the active sites (i.e., Mg^{2+} species) of urea hydrolysis MMOs.

3.4.2 CO_2 Adsorption Kinetics

Figure 12 shows the CO_2 adsorption capacity *versus* time (minutes) profile of MMOs derived by the LDHs synthesized by the urea hydrolysis and co-precipitation method to evaluate the effects of the synthesis method and metal salts precursors on the CO_2 sorption kinetics of MMOs. The absence of a clear plateau in all sorption profiles after 120 min shows the nonequilibrium adsorption behavior of CO_2 in the LDH-derived MMOs sorbents. The vast difference in the uptake slopes of these profiles suggests two different kinetic regimes: a steep increase in the first few minutes of adsorption (fast reaction) followed by a small increase until the end of the adsorption step (slow reaction). In a cyclic adsorption operation, the fast reaction is often the desired reaction as it mostly occurs on the sorbent surface and requires lower heat of adsorption (Ebner et al., 2006, 2007; Walspurger et al., 2010; Du et al., 2011). In contrast, the slow reaction is generally not favored and forms bulk $MgCO_3$ species, which tend to be difficult to regenerate and cause process issues such as poor mechanical stability and CO_2 slip through the adsorption bed (Jansen et al., 2013).

Overall, the co-precipitated MMOs clearly have better CO_2 adsorption kinetics than urea hydrolysis MMOs. The better kinetics of co-precipitated MMOs seem to be directly linked to the sodium content of samples that give higher CO_2 uptakes in the fast reaction step. For example, MMOs that achieved the highest CO_2 uptake in the fast reaction step are CPNI2, followed by CPNI3, CPNI4, CPCL3, CPCL4, and CPCL2, following the same order as the one with the highest concentration of sodium present in **Figure 6**. For the urea hydrolysis MMOs, the UHNI2 sample shows remarkably higher CO_2 uptake than the rest of its kind during the fast reaction step. This is likely due to the combined effects of high LDH purity of the sample and

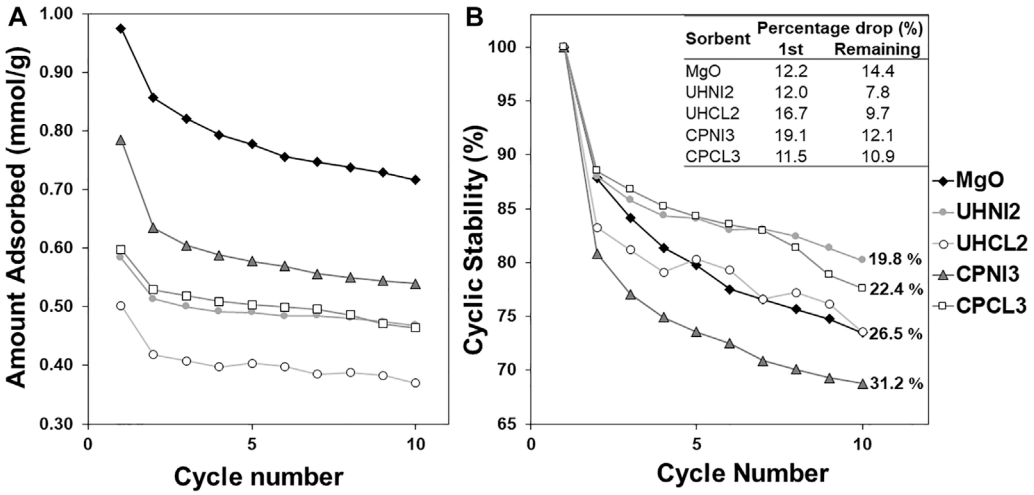

FIGURE 13 | (A) CO_2 adsorption capacity and **(B)** percentage reduction in adsorption capacity by cycles of selected MMOs synthesized with the urea hydrolysis and co-precipitation methods.

additional sodium content from the precursor metal nitrates, which provided more active sites for CO_2 adsorption.

In the slow reaction step, all urea hydrolysis MMOs show similar kinetics, except for the UHCL2 MMOs with an obvious steeper profile, suggesting a higher carbonation rate. As the slow reaction corresponds to the formation of bulk $MgCO_3$ species, this higher uptake by the UHCL2 sample is likely to do with its higher Mg content, as a result of a high LDH purity and high observed Mg/Al ratio (**Table 4**), which provided more Mg-O sites for the carbonation reaction. This is the same as co-precipitated MMOs, where the samples with higher Mg/Al ratios (i.e., 3 and 4) show higher carbonation rates in the slow reaction step compared to the lower ones (i.e., CPCL2 and CPNI2).

For the co-precipitation and urea hydrolysis methods, MMOs synthesized from metal nitrates tend to show better CO_2 kinetics than the ones synthesized from metal chlorides by having higher CO_2 uptakes in the fast reaction step. For the slow reaction step, no obvious effect due to the choice of metal salt precursors is seen. Overall, the sodium content of the sample seems to have a direct positive impact on the CO_2 adsorption kinetics of LDH-derived MMOs.

3.4.3 Cyclic Stability

Cyclic CO_2 adsorption tests were carried out to test the cyclic stability of selected LDH-derived MMOs sorbents and compared with pure magnesium oxide (MgO, obtained by calcining $Mg(OH)_2$ at 400°C for 4 h), which serves as the reference case. MgO is a suitable benchmark to assess the cyclic stability of LDH-derived MMOs because the MMOs sorbents were originally proposed as an alternative option to MgO, which was found to have poor cyclic stability in general. Only four MMOs were selected to study for cyclic tests based on three criteria: 1) highest LDH yields, 2) good agreement between expected and observed Mg/Al ratios, and 3) adequate CO_2 adsorption capacities. Note that the adsorption and desorption were carried out for 30 min each. **Figure 13** shows the CO_2 adsorption capacities of tested MMOs sorbents in each cycle and the percentage reduction in CO_2 sorption capacities calculated with respect to the amount adsorbed in the first cycle.

Figure 13A shows that all LDH-derived MMOs and MgO sorbents show a slow gradual drop in CO_2 adsorption capacities over 10 adsorption cycles and there is no obvious plateau, which means the capacities might reduce further. A similar trend is observed in **Figure 13B**, which shows the percentage drop of adsorption capacities calculated with respect to the first cycle. It seems that all the sorbents experience the largest drop in the adsorption capacities after the first cycle. No obvious correlation from either the synthesis method or metal salts precursors affects this large initial drop in adsorption capacities. Among the MMO samples, **Figure 13A** shows that CPNI3 sample presents the highest CO_2 adsorption capacities in all 10 cycles. Interestingly, despite the promising outlook of CPNI3, a close look in **Figure 13B** can find that, in fact, the same sorbent shows the largest reduction in overall cyclic stability (31.2%) and is the only MMOs sorbent performing worse than MgO sorbent (26.5%). On the contrary, the urea hydrolysis samples show relative good cyclic performance than their co-precipitated counterparts, as their CO_2 adsorption capacities after the first cycles are almost similar in **Figure 13A**. Overall, LDH-based MMOs appear to have better cyclic stability than pure MgO sorbent (i.e., lower percentage loss in CO_2 adsorption capacities after the first cycle).

3.4.4 Comparison With Literature LDH-Derived MMOs

A performance comparison at 200°C of MMOs synthesized in this work with relevant analogs previously reported in the literature is shown in **Figure 14** (Ding and Alpay, 2001; Yong et al., 2001; Ram Reddy et al., 2006; Lee et al., 2010; Wang et al., 2012; Gao et al., 2013; Jang et al., 2014; Kou et al., 2018; Megías-Sayago et al., 2019; Liu et al., 2020). In **Figure 14**, MMOs refer to those derived from pristine Mg-Al-CO_3 LDHs, unless otherwise specified (e.g., Mg-Al-stearate and Mg-Al-SDS). Those MMOs

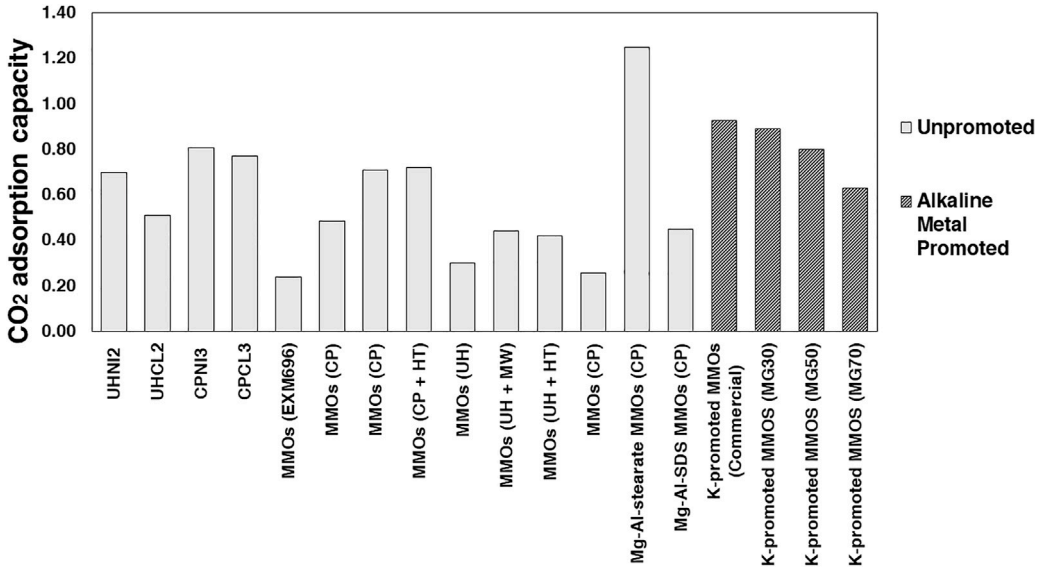

FIGURE 14 | CO_2 adsorption capacities of MMOs synthesized in the present work and those previously reported. The grey bars indicate MMOs derived from unpromoted Mg-Al-LDHs, whereas dark bars represent MMOs derived from alkali-metal promoted Mg-Al-LDHs.

investigated at other conditions for different applications (>300°C and elevated pressures) are excluded. Commercial LDH-based MMOs sorbents were also included as benchmark materials, even though some have been promoted with alkali metal carbonates and salts, such as K_2CO_3, KNO_3, and $NaNO_3$. Full details of these MMOs and the adsorption conditions (e.g., synthesis method employed, temperature, CO_2 partial pressure) are summarized in **Supplementary Table S1**. As shown in **Figure 14**, the CO_2 adsorption capacities of MMOs synthesized in this work are lower than those promoted with alkali metal salts and carbonates. However, the capture capacities are still better than most of the MMOs derived from unpromoted Mg-Al LDHs, except for one MMOs derived from Mg-Al-stearate LDHs, which have been modified for larger surface area and smaller particle sizes.

Overall, this work shows that selecting a good CO_2 capture material does not just rely on its CO_2 adsorption performance. Other factors are equally important such as productivity, environmental sustainability, cyclic stability, and efficiency of the overall synthetic process, including the generation of waste (i.e., effluents). For example, nitrate precursors tend to be more costly than the chloride ones, and they might also have disposal issues due to the ecologically unsafe nitrate ions generated in the effluents. However, it is hard to conclude which synthesis method or which metal salt precursors are more superior, unless a completed life cycle assessment (LCA) is carried out.

4 CONCLUSION

The selection of the appropriate synthesis method and salt precursors is a crucial decision in developing a CO_2 capture adsorbent. In the present study, the impact of the synthesis method and choice of salt precursors on the chemical composition of LDHs was investigated. Additionally, the CO_2 adsorption behavior of Mg-Al-LDH-based MMOs was studied, and its relationship with synthesis efficiency metrics (e.g., purity, synthesis yields, and percentage of unreacted reactants) was established.

LDHs synthesized by the urea hydrolysis method showed higher Al^{3+} substitution (a = 3.032–3.038 Å) and higher amorphous Al-phases as impurities, resulting in low-purity LDHs. The synthesis yield was relatively low (51%–82%), and a high percentage of unreacted Mg^{2+} ions was found in the reaction filtrates. In contrast, LDHs synthesized *via* co-precipitation showed more varied compositions (a = 3.037–3.069 Å), which were in close agreement with the targeted ones at synthesis. The synthesis yields were close to 100% in all the samples, and negligible amounts of metal ions were found in the filtrates. All the samples showed trace amounts of sodium (0.04%–0.9 wt%), which are likely to originate from the precursor employed. Metal chlorides were a better precursor for efficient precipitation of LDHs compared to metal nitrates for both co-precipitation and urea hydrolysis methods.

The resultant MMOs showed different textural properties. MMOs generated from the urea hydrolysis method show large hexagonal crystallites, whereas MMOs generated from co-precipitation show large aggregates of irregular shapes.

The presence of impure phases and the sodium content significantly affect the CO_2 adsorption capacities of LDH-derived MMOs. The highest CO_2 uptakes were measured for MMOs derived from urea hydrolysis samples (0.70 mmol/g), exhibiting the highest LDH yield and lowest amounts of Al-based impurities, and from co-precipitated LDH-derived MMO samples (0.81 mmol/g) with the highest sodium content. The impact of the synthesis method and metal salt precursors on the CO_2 adsorption kinetics of LDH-derived MMOs was also demonstrated. MMOs synthesized

by the co-precipitation method and metal nitrates have better CO_2 sorption kinetics than those synthesized by the urea hydrolysis method and metal chlorides. Most MMOs sorbent was found to have better cyclic stability than pure MgO sorbent, although their sorption capacities are lower.

DATA AVAILABILITY STATEMENT

The original contributions presented in the study are included in the article/**Supplementary Material**, further inquiries can be directed to the corresponding author.

AUTHOR CONTRIBUTIONS

LC, GM, and SG: conceptualization and design of the study. LC: experiments, acquisition and interpretation of data, visualization, and writing of the first draft of the manuscript. GM and SG: writing—review and editing for important intellectual content. SG and MM-V: supervision, project administration, and funding acquisition. All authors contributed to manuscript revision and read and approved the submitted version.

FUNDING

The authors gratefully acknowledge the financial support from Engineering and Physical Sciences Research Council (EP/N024540/1), James Watt Scholarship from Heriot-Watt University, and the PrISMa project. The PrISMa Project (no. 299659) is funded through the ACT programme (Accelerating CCS Technologies, Horizon 2020 Project no. 294766). Financial contributions were from the Department for Business, Energy and Industrial Strategy (BEIS) together with extra funding from NERC and EPSRC Research Councils, United Kingdom. The Research Council of Norway (RCN), Norway; Swiss Federal Office of Energy (SFOE), Switzerland; and US-Department of Energy (US-DOE), United States, are gratefully acknowledged. Additional financial support from TOTAL and Equinor is also gratefully acknowledged.

SUPPLEMENTARY MATERIAL

The Supplementary Material for this article can be found online at: https://www.frontiersin.org/articles/10.3389/fenrg.2022.882182/full#supplementary-material

REFERENCES

Abanades, J. C., Arias, B., Lyngfelt, A., Mattisson, T., Wiley, D. E., Li, H., et al. (2015). Emerging CO2 Capture Systems. *Int. J. Greenhouse Gas Control.* 40, 126–166. doi:10.1016/j.ijggc.2015.04.018

Adachi-Pagano, M., Forano, C., and Besse, J.-P. (2003). Synthesis of Al-Rich Hydrotalcite-like Compounds by Using the Urea Hydrolysis Reaction-Control of Size and Morphology. *J. Mater. Chem.* 13, 1988–1993. doi:10.1039/b302747n

Allmann, R., and Jepsen, H. P. (1969). Die struktur des hydrotalkits. *Neues Jahrbuch für Mineralogie Monatshefte* 1969, 544Â551.

Arco, M. D., Malet, P., Trujillano, R., and Rives, V. (1999). Synthesis and Characterization of Hydrotalcites Containing Ni(II) and Fe(III) and Their Calcination Products. *Chem. Mater.* 11, 624–633. doi:10.1021/cm9804923

Arstad, B., Blom, R., Håkonsen, S. F., Pierchala, J., Cobden, P., Lundvall, F., et al. (2020). Synthesis and Evaluation of K-Promoted $Co_{3-x}Mg_xAl$-Oxides as Solid CO_2 Sorbents in the Sorption-Enhanced Water–Gas Shift (SEWGS) Reaction. *Ind. Eng. Chem. Res.* 59, 17837–17844. doi:10.1021/acs.iecr.0c02322

Benito, P., Labajos, F. M., and Rives, V. (2006). Uniform Fast Growth of Hydrotalcite-like Compounds. *Cryst. Growth Des.* 6, 1961–1966. doi:10.1021/cg0506222

Boclair, J. W., and Braterman, P. S. (1999). Layered Double Hydroxide Stability. 1. Relative Stabilities of Layered Double Hydroxides and Their Simple Counterparts. *Chem. Mater.* 11, 298–302. doi:10.1021/cm980523u

Brindley, G. W., and Kikkawa, S. (1979). A crystal-chemical Study of Mg,Al and Ni,N Hydroxy-Perchlorates and Hydroxy-Carbonates. *Am. Mineral.* 64, 836–843.

Cadars, S., Layrac, G., Gérardin, C., Deschamps, M., Yates, J. R., Tichit, D., et al. (2011). Identification and Quantification of Defects in the Cation Ordering in Mg/Al Layered Double Hydroxides. *Chem. Mater.* 23, 2821–2831. doi:10.1021/cm200029q

Cavani, F., Trifirò, F., and Vaccari, A. (1991). Hydrotalcite-type Anionic Clays: Preparation, Properties and Applications. *Catal. Today* 11, 173–301. doi:10.1016/0920-5861(91)80068-k

Chanburanasiri, N., Ribeiro, A. M., Rodrigues, A. E., Laosiripojana, N., and Assabumrungrat, S. (2013). Simulation of Methane Steam Reforming Enhanced by *In Situ* CO_2 Sorption Using K_2CO_3-Promoted Hydrotalcites for H_2 Production. *Energy Fuels* 27, 4457–4470. doi:10.1021/ef302043e

Cheah, L. A., Manohara, G. V., Maroto-Valer, M. M., and Garcia, S. (2020). Layered Double Hydroxide (LDH)-Derived Mixed Metal Oxides (MMOs): A Systematic Crystal-Chemical Approach to Investigating the Chemical Composition and its Effect on High Temperature CO_2 Capture. *ChemistrySelect* 5, 5587–5594. doi:10.1002/slct.201904447

Costantino, U., Marmottini, F., Nocchetti, M., and Vivani, R. (1998). New Synthetic Routes to Hydrotalcite-Like Compounds – Characterisation and Properties of the Obtained Materials. *Eur. J. Inorg. Chem.* 1998, 1439–1446. doi:10.1002/(sici)1099-0682(199810)1998:10<1439::aid-ejic1439>3.0.co;2-1

Cross, H. E., and Brown, D. R. (2010). Entrained Sodium in Mixed Metal Oxide Catalysts Derived from Layered Double Hydroxides. *Catal. Commun.* 12, 243–245. doi:10.1016/j.catcom.2010.09.008

Cunha, A. F., Wu, Y. J., Díaz Alvarado, F. A., Santos, J. C., Vaidya, P. D., and Rodrigues, A. E. (2012). Steam Reforming of Ethanol on a Ni/Al_2O_3 Catalyst Coupled with a Hydrotalcite-like Sorbent in a Multilayer Pattern for Co_2 Uptake. *Can. J. Chem. Eng.* 90, 1514–1526. doi:10.1002/cjce.20662

Dijkstra, J. W., Walspurger, S., Elzinga, G. D., Pieterse, J. A. Z., Boon, J., and Haije, W. G. (2018). Evaluation of Postcombustion CO_2 Capture by a Solid Sorbent with Process Modeling Using Experimental CO_2 and H_2O Adsorption Characteristics. *Ind. Eng. Chem. Res.* 57, 1245–1261. doi:10.1021/acs.iecr.7b03552

Ding, Y., and Alpay, E. (2001). High Temperature Recovery of CO_2 from Flue Gases Using Hydrotalcite Adsorbent. *Process Saf. Environ. Prot.* 79, 45–51. doi:10.1205/095758201531130

Drage, T. C., Snape, C. E., Stevens, L. A., Wood, J., Wang, J., Cooper, A. I., et al. (2012). Materials Challenges for the Development of Solid Sorbents for Post-Combustion Carbon Capture. *J. Mater. Chem.* 22, 2815–2823. doi:10.1039/C2JM12592G

Du, H., Ebner, A. D., and Ritter, J. A. (2011). Pressure Dependence of the Nonequilibrium Kinetic Model that Describes the Adsorption and Desorption Behavior of CO_2 in K-Promoted Hydrotalcite Like Compound. *Ind. Eng. Chem. Res.* 50, 412–418. doi:10.1021/ie100965b

Dutcher, B., Fan, M., and Russell, A. G. (2015). Amine-Based CO_2 Capture Technology Development from the Beginning of 2013-A Review. *ACS Appl. Mater. Inter.* 7, 2137–2148. doi:10.1021/am507465f

Ebner, A. D., Reynolds, S. P., and Ritter, J. A. (2006). Understanding the Adsorption and Desorption Behavior of CO_2 on a K-Promoted Hydrotalcite-like Compound (HTlc) through Nonequilibrium Dynamic Isotherms. *Ind. Eng. Chem. Res.* 45, 6387–6392. doi:10.1021/ie060389k

Ebner, A. D., Reynolds, S. P., and Ritter, J. A. (2007). Nonequilibrium Kinetic Model that Describes the Reversible Adsorption and Desorption Behavior of CO_2 in a K-Promoted Hydrotalcite-like Compound. *Ind. Eng. Chem. Res.* 46, 1737–1744. doi:10.1021/ie061042k

Fang, X., Men, Y., Wu, F., Zhao, Q., Singh, R., Xiao, P., et al. (2019). Promoting CO_2 Hydrogenation to Methanol by Incorporating Adsorbents into Catalysts: Effects of Hydrotalcite. *Chem. Eng. J.* 378, 122052. doi:10.1016/j.cej.2019.122052

Forano, C., Costantino, U., Prévot, V., and Gueho, C. T. (2013). Layered Double Hydroxides (LDH). *Dev. Clay Sci.* 5, 745–782. doi:10.1016/B978-0-08-098258-8.00025-0

Gao, Y., Zhang, Z., Wu, J., Yi, X., Zheng, A., Umar, A., et al. (2013). Comprehensive Investigation of CO_2 Adsorption on Mg-Al-CO_3 LDH-Derived Mixed Metal Oxides. *J. Mater. Chem. A.* 1, 12782–12790. doi:10.1039/c3ta13039h

Gastuche, M. C., Brown, G., and Mortland, M. M. (1967). Mixed Magnesium-Aluminium Hydroxides. I. Preparation and Characterization of Compounds Formed in Dialysed Systems. *Clay miner.* 7, 177–192. doi:10.1180/claymin.1967.007.2.05

Glier, J. C., and Rubin, E. S. (2013). Assessment of Solid Sorbents as a Competitive post-combustion CO_2 Capture Technology. *Energ. Proced.* 37, 65–72. Elsevier Ltd. doi:10.1016/j.egypro.2013.05.086

Hanif, A., Sun, M., Shang, S., Tian, Y., Yip, A. C. K., Ok, Y. S., et al. (2019). Exfoliated Ni-Al LDH 2D Nanosheets for Intermediate Temperature CO_2 Capture. *J. Hazard. Mater.* 374, 365–371. doi:10.1016/j.jhazmat.2019.04.049

Hazen, R. M. (1976). Effects of Temperature and Pressure on the Cell Dimension and X-ray Temperature Factors of Periclase. *Am. Mineral.* 61, 266–271.

He, J., Wei, M., Li, B., Kang, Y., Evans, D. G., and Duan, X. (2005). Preparation of Layered Double Hydroxides. *Struct. Bond.* 119, 89–119. doi:10.1007/430_006

Hernandez-Moreno, M. J., Ulibarri, M. A., Rendon, J. L., and Serna, C. J. (1985). IR Characteristics of Hydrotalcite-like Compounds. *Phys. Chem. Miner.* 12, 34–38.

Hibino, T., and Ohya, H. (2009). Synthesis of Crystalline Layered Double Hydroxides: Precipitation by Using Urea Hydrolysis and Subsequent Hydrothermal Reactions in Aqueous Solutions. *Appl. Clay Sci.* 45, 123–132. doi:10.1016/j.clay.2009.04.013

IPCC (2018). *Global Warming of 1.5°C*. Geneva, Switzerland: The Intergovernmental Panel on Climate Change (IPCC). An IPCC Special Report on the impacts of global warming of 1.5°C above pre-industrial levels and related global greenhouse gas emission pathways, in the context of strengthening the global response to the threat of climate change, sustainable development, and efforts to eradicate poverty.

Iruretagoyena, D., Shaffer, M. S. P., and Chadwick, D. (2015). Layered Double Oxides Supported on Graphene Oxide for CO2 Adsorption: Effect of Support and Residual Sodium. *Ind. Eng. Chem. Res.* 54, 6781–6792. doi:10.1021/acs.iecr.5b01215

Jang, H. J., Lee, C. H., Kim, S., Kim, S. H., and Lee, K. B. (2014). Hydrothermal Synthesis of K2CO3-promoted Hydrotalcite from Hydroxide-form Precursors for Novel High-Temperature CO2 Sorbent. *ACS Appl. Mater. Inter.* 6, 6914–6919. doi:10.1021/am500720f

Jansen, D., van Selow, E., Cobden, P., Manzolini, G., Macchi, E., Gazzani, M., et al. (2013). SEWGS Technology Is Now Ready for Scale-Up! *Energ. Proced.* 37, 2265–2273. doi:10.1016/j.egypro.2013.06.107

Jobbágy, M., and Regazzoni, A. E. (2011). Dissolution of Nano-Size Mg-Al-Cl Hydrotalcite in Aqueous media. *Appl. Clay Sci.* 51, 366–369. doi:10.1016/j.clay.2010.11.027

Johnson, C. A., and Glasser, F. P. (2003). Hydrotalcite-like Minerals (M2Al(OH)6(CO3)0.5.XH2O, where M = Mg, Zn, Co, Ni) in the Environment: Synthesis, Characterization and Thermodynamic Stability. *Clays Clay Miner.* 51, 1–8. doi:10.1346/CCMN.2003.510101

Kaneyoshi, M., and Jones, W. (1999). Formation of Mg-Al Layered Double Hydroxides Intercalated with Nitrilotriacetate Anions. *J. Mater. Chem.* 9, 805–811. doi:10.1039/a808415g

Keeling, C. D., Bacastow, R. B., Bainbridge, A. E., Ekdahl, C. A., Jr, Guenther, P. R., Waterman, L. S., et al. (1976). Atmospheric Carbon Dioxide Variations at Mauna Loa Observatory, Hawaii. *Tellus* 28, 538–551. doi:10.3402/tellusa.v28i6.11322

Kou, X., Guo, H., Ayele, E. G., Li, S., Zhao, Y., Wang, S., et al. (2018). Adsorption of CO_2 on MgAl-CO3 LDHs-Derived Sorbents with 3D Nanoflower-like Structure. *Energy Fuels* 32, 5313–5320. doi:10.1021/acs.energyfuels.8b00024

Kukkadapu, R. K., Witkowski, M. S., and Amonette, J. E. (1997). Synthesis of a Low-Carbonate High-Charge Hydrotalcite-like Compound at Ambient Pressure and Atmosphere. *Chem. Mater.* 9, 417–419. doi:10.1021/cm960536c

Lee, J. M., Min, Y. J., Lee, K. B., Jeon, S. G., Na, J. G., and Ryu, H. J. (2010). Enhancement of CO2Sorption Uptake on Hydrotalcite by Impregnation with K2CO3. *Langmuir* 26, 18788–18797. doi:10.1021/la102974s

Liu, Q., Zhao, Y., Jiang, Z., Cui, Y., Wang, J., and Ai, N. (2020). Computational and Experimental Studies on the CO2 Adsorption of Layered Double Hydroxide Intercalated by Anionic Surfactant. *Appl. Clay Sci.* 190, 105556. doi:10.1016/j.clay.2020.105556

Marappa, S., and Kamath, P. V. (2015). Structure of the Carbonate-Intercalated Layered Double Hydroxides: A Reappraisal. *Ind. Eng. Chem. Res.* 54, 11075–11079. doi:10.1021/acs.iecr.5b03207

Martins, J. A., Faria, A. C., Soria, M. A., Miguel, C. V., Rodrigues, A. E., and Madeira, L. M. (2019). Co2 Methanation over Hydrotalcite-Derived Nickel/ruthenium and Supported Ruthenium Catalysts. *Catalysts* 9, 1008. doi:10.3390/catal9121008

Mascolo, G., and Marino, O. (1980). A New Synthesis and Characterization of Magnesium-Aluminium Hydroxides. *Mineral. Mag.* 43, 619–621. doi:10.1180/MINMAG.1980.043.329.09

Megías-Sayago, C., Bingre, R., Huang, L., Lutzweiler, G., Wang, Q., and Louis, B. (2019). CO_2 Adsorption Capacities in Zeolites and Layered Double Hydroxide Materials. *Front. Chem.* 7, 1–10. doi:10.3389/fchem.2019.00551

Mills, S. J., Christy, A. G., Génin, J.-M. R., Kameda, T., and Colombo, F. (2012). Nomenclature of the Hydrotalcite Supergroup: Natural Layered Double Hydroxides. *Mineral. Mag.* 76, 1289–1336. doi:10.1180/minmag.2012.076.5.10

Miyata, S., and Kumura, T. (1973). Synthesis of New Hydrotalcite-like Compounds and Their Physico-Chemical Properties. *Chem. Lett.* 2, 843–848. doi:10.1246/cl.1973.843

Miyata, S. (1980). Physico-Chemical Properties of Synthetic Hydrotalcites in Relation to Composition. *Clays Clay Miner.* 28, 50–56. doi:10.1346/ccmn.1980.0280107

Ozsa, P. M., Mehta, S. H., Sheth, M. V., Ghosh, P. K., Gandhi, M. R., and Chunawala, J. R. (2006). *Process for Preparing Hydrotalcite and Brucite Type Posite Charged Layers*. U.S. Patent No 7,022,302. Washington, DC: U.S. Patent and Trademark Office.

Pausch, I., Lohse, H.-H., Schurmann, K., and Allmann, R. (1986). Syntheses of Disordered and Al-Rich Hydrotalcite-Like Compounds. *Clays Clay Miner.* 34, 507–510. doi:10.1346/ccmn.1986.0340502

Prinetto, F., Ghiotti, G., Graffin, P., and Tichit, D. (2000). Synthesis and Characterization of Sol-Gel Mg/Al and Ni/Al Layered Double Hydroxides and Comparison with Co-precipitated Samples. *Microporous Mesoporous Mater.* 39, 229–247. doi:10.1016/S1387-1811(00)00197-9

Radha, A. V., and Kamath, P. V. (2003). Aging of Trivalent Metal Hydroxide/Oxide Gels in Divalent Metal Salt Solutions: Mechanism of Formation of Layered Double Hydroxides (LDHs). *Bull. Mater. Sci.* 26, 661–666. doi:10.1007/bf02706760

Radha, A. V., Kamath, P. V., and Shivakumara, C. (2007). Order and Disorder Among the Layered Double Hydroxides: Combined Rietveld and DIFFaX Approach. *Acta Crystallogr. Sect B* 63, 243–250. doi:10.1107/s010876810700122x

Ram Reddy, M. K., Xu, Z. P., Lu, G. Q., and Diniz da Costa, J. C. (2006). Layered Double Hydroxides for CO2 Capture: Structure Evolution and Regeneration. *Ind. Eng. Chem. Res.* 45, 7504–7509. doi:10.1021/ie060757k

Richardson, I. G. (2013). The Importance of Proper crystal-chemical and Geometrical Reasoning Demonstrated Using Layered Single and Double Hydroxides. *Acta Crystallogr. Sect B* 69, 150–162. doi:10.1107/S205251921300376X

Rocha, J., del Arco, M., Rives, V., and Ulibarri, M. A. (1999). Reconstruction of Layered Double Hydroxides from Calcined Precursors: a Powder XRD and 27Al MAS NMR Study. *J. Mater. Chem.* 9, 2499–2503. doi:10.1039/A903231B

Selow, E. R. V., Cobden, P. D., Verbraeken, P. A., Hufton, J. R., and van den Brink, R. W. (2009). Carbon Capture by Sorption-Enhanced Water–Gas Shift Reaction Process Using Hydrotalcite-Based Material. *Ind. Eng. Chem. Res.* 48, 4184–4193. doi:10.1021/ie801713a

Seron, A., and Delorme, F. (2008). Synthesis of Layered Double Hydroxides (LDHs) with Varying pH: A Valuable Contribution to the Study of Mg/Al LDH Formation Mechanism. *J. Phys. Chem. Sol.* 69, 1088–1090. doi:10.1016/J.JPCS.2007.10.054

Sheldon, R. A. (2018). Metrics of Green Chemistry and Sustainability: Past, Present, and Future. *ACS Sustain. Chem. Eng.* 6, 32–48. doi:10.1021/acssuschemeng.7b03505

Sjostrom, S., and Krutka, H. (2010). Evaluation of Solid Sorbents as a Retrofit Technology for CO2 Capture. *Fuel* 89, 1298–1306. doi:10.1016/j.fuel.2009.11.019

Theiss, F. L., Ayoko, G. A., and Frost, R. L. (2016). Synthesis of Layered Double Hydroxides Containing Mg^{2+} , Zn^{2+} , Ca^{2+} and Al^{3+} Layer Cations by Co-precipitation Methods - A Review. *Appl. Surf. Sci.* 383, 200–213. doi:10.1016/j.apsusc.2016.04.150

Tichit, D., Layrac, G., and Gérardin, C. (2019). Synthesis of Layered Double Hydroxides through Continuous Flow Processes: A Review. *Chem. Eng. J.* 369, 302–332. doi:10.1016/j.cej.2019.03.057

van Dijk, H. A. J., Walspurger, S., Cobden, P. D., van den Brink, R. W., and de Vos, F. G. (2011). Testing of Hydrotalcite-Based Sorbents for CO_2 and H_2S Capture for Use in Sorption Enhanced Water Gas Shift. *Int. J. Greenhouse Gas Control.* 5, 505–511. doi:10.1016/j.ijggc.2010.04.011

Vyalikh, A., Massiot, D., and Scheler, U. (2009). Structural Characterisation of Aluminium Layered Double Hydroxides by 27Al Solid-State NMR. *Solid State. Nucl. Magn. Reson.* 36, 19–23. doi:10.1016/J.SSNMR.2009.04.002

Walspurger, S., Cobden, P. D., Safonova, O. V., Wu, Y., and Anthony, E. J. (2010). High CO_2 Storage Capacity in Alkali-Promoted Hydrotalcite-Based Material: *In Situ* Detection of Reversible Formation of Magnesium Carbonate. *Chem. - A Eur. J.* 16, 12694–12700. doi:10.1002/chem.201000687

Wang, Q., Tay, H. H., Zhong, Z., Luo, J., and Borgna, A. (2012). Synthesis of High-Temperature CO_2 Adsorbents from Organo-Layered Double Hydroxides with Markedly Improved CO_2 Capture Capacity. *Energ. Environ. Sci.* 5, 7526–7530. doi:10.1039/c2ee21409a

Wang, J., Huang, L., Yang, R., Zhang, Z., Wu, J., Gao, Y., et al. (2014). Recent Advances in Solid Sorbents for CO_2 Capture and New Development Trends. *Energy Environ. Sci.* 7, 3478–3518. doi:10.1039/c4ee01647e

Yong, Z., Mata, V., and Rodrigues, A. E. (2001). Adsorption of Carbon Dioxide onto Hydrotalcite-like Compounds (HTlcs) at High Temperatures. *Ind. Eng. Chem. Res.* 40, 204–209. doi:10.1021/ie000238w

Zhang, F., Lu, B., and Sun, P. (2020). Highly Stable Ni-Based Catalysts Derived from LDHs Supported on Zeolite for CO2 Methanation. *Int. J. Hydrogen Energ.* 45, 16183–16192. doi:10.1016/j.ijhydene.2020.04.099

Conflict of Interest: The authors declare that the research was conducted in the absence of any commercial or financial relationships that could be construed as a potential conflict of interest.

Publisher's Note: All claims expressed in this article are solely those of the authors and do not necessarily represent those of their affiliated organizations or those of the publisher, the editors, and the reviewers. Any product that may be evaluated in this article, or claim that may be made by its manufacturer, is not guaranteed or endorsed by the publisher.